



**Environmental
Science**
Processes & Impacts

**The Sea Spray Chemistry and Particle Evolution Study
(SeaSCAPE): Overview and Experimental Methods**

| | |
|---------------|---|
| Journal: | <i>Environmental Science: Processes & Impacts</i> |
| Manuscript ID | EM-ART-07-2021-000260.R1 |
| Article Type: | Paper |
| | |

SCHOLARONE™
Manuscripts

The Sea Spray Chemistry and Particle Evolution Study (SeaSCAPE): Overview and Experimental Methods

Jon S. Sauer^{1†}, Kathryn J. Mayer^{1†}, Christopher Lee^{2†}, Michael R. Alves¹, Sarah Amiri^{2,3}, Cristina J. Bahaveolos⁴, Emily B. Franklin⁵, Daniel R. Crocker¹, Duyen Dang¹, Julie Dinasquet², Lauren A. Garofalo⁶, Chathuri P. Kaluarachchi⁷, Delaney B. Kilgour⁴, Liora E. Mael¹, Brock A. Mitts¹, Daniel R. Moon^{8,9}, Alexia N. Moore¹, Clare K. Morris², Catherine A. Mullenmeister¹, Chi-Min Ni⁴, Matthew A. Pendergraft², Daniel Petras^{2,10}, Rebecca M. C. Simpson², Stephanie Smith², Paul R. Tumminello¹, Joseph L. Walker², Paul J. DeMott¹¹, Delphine K. Farmer⁶, Allen H. Goldstein^{5,12}, Vicki H. Grassian^{1,2,13}, Jules S. Jaffe², Francesca Malfatti^{2,14}, Todd R. Martz², Jonathan H. Slade¹, Alexei V. Tivanski⁷, Timothy H. Bertram⁴, Christopher D. Cappa⁸, Kimberly A. Prather^{*1,2}

1. Department of Chemistry and Biochemistry, University of California, San Diego, La Jolla, California 92093, United States
2. Scripps Institution of Oceanography, University of California, San Diego, La Jolla, California 92093, United States
3. Marine Science Institute, University of California, Santa Barbara, Santa Barbara, California 93106, United States
4. Department of Chemistry, University of Wisconsin, Madison, Wisconsin 53706, United States
5. Department of Civil and Environmental Engineering, University of California, Berkeley, California 94720, United States
6. Department of Chemistry, Colorado State University, Fort Collins, Colorado 80523, United States
7. Department of Chemistry, University of Iowa, Iowa City, Iowa 52242, United States
8. Department of Civil and Environmental Engineering, University of California, Davis, California 95616, United States
9. Institute for Chemical Science, Heriot-Watt University, Edinburgh EH14 4AS, United Kingdom
10. Skaggs School of Pharmacy and Pharmaceutical Science, University of California, San Diego, La Jolla, California 92093, United States
11. Department of Atmospheric Sciences, Colorado State University, Fort Collins, Colorado 80523, United States
12. Department of Environmental Science, Policy and Management, University of California, Berkeley, California 94720, United States
13. Department of Nanoengineering, University of California San Diego, La Jolla, California 92093, United States
14. Università degli Studi di Trieste, Department of Life Sciences, Trieste, 34127, Italy

Environmental Science: Processes and Impacts

2021

Correspondence to: Kimberly A. Prather (kprather@ucsd.edu)

†Authors contributed equally.

Abstract

Marine aerosols strongly influence climate through their interactions with solar radiation and clouds. However, significant questions remain regarding the influences of biological activity and seawater chemistry on the flux, chemical composition, and climate-relevant properties of marine aerosols and gases. Wave channels, a traditional tool of physical oceanography, have been adapted for large-scale ocean-atmosphere mesocosm experiments in the laboratory. These experiments enable the study of aerosols under controlled conditions which isolate the marine system from atmospheric anthropogenic and terrestrial influences. Here, we present an overview of the 2019 Sea Spray Chemistry and Particle Evolution (SeaSCAPE) study, which was conducted in an 11,800 L wave channel which was modified to facilitate atmospheric measurements. The SeaSCAPE campaign sought to determine the influence of biological activity in seawater on the production of primary sea spray aerosols, volatile organic compounds (VOCs), and secondary marine aerosols. Notably, the SeaSCAPE experiment also focused on understanding how photooxidative aging processes transform the composition of marine aerosols. In addition to a broad range of aerosol, gas, and seawater measurements, we present key results which highlight the experimental capabilities during the campaign, including the phytoplankton bloom dynamics, VOC production, and the effects of photochemical aging on aerosol production, morphology, and chemical composition. Additionally, we discuss the modifications made to the wave channel to improve aerosol production and reduce background contamination, as well as subsequent characterization experiments. The SeaSCAPE experiment provides unique insight into the connections between marine biology, atmospheric chemistry, and climate-relevant aerosol properties, and demonstrates how an ocean-atmosphere-interaction facility can be used to isolate and study reactions in the marine atmosphere in the laboratory under more controlled conditions.

Environmental Significance Statement

The ocean-atmosphere system influences Earth's radiative balance, cloud formation and precipitation, and air quality, all of which directly impact human health and well-being. Laboratory control experiments play a key role in improving our understanding of the marine atmosphere and allow for measurements of aerosols and gases under clean, isolated, and environmentally relevant conditions. Here, we describe the design and operation of an 11,800 L wave channel for replicating the ocean-atmosphere environment, with specific details provided on the production of representative sea spray aerosols, marine microbiology, biogenic gases, and secondary marine aerosols. The findings presented herein demonstrate best experimentation practices and illustrate challenges that exist when working to replicate and ultimately understand chemical reactions and biology feedbacks in the ocean-atmosphere system.

1. Introduction

Oceans cover 71% of Earth's surface and are a major source of both aerosols and trace gases, which affect climate, air quality, and human health. Aerosols influence climate directly by absorbing and scattering solar radiation, and indirectly by serving as cloud condensation nuclei (CCN) and ice nucleating particles (INPs), thus affecting the properties of clouds. The interactions between aerosols and clouds represent one of the largest uncertainties in estimates of Earth's radiative budget.^{1,2} Constraining the flux, composition, and cloud-relevant properties of marine aerosols is crucial for understanding their influence on atmospheric processes and establishing past and future changes in the climate system.

Sea spray aerosol (SSA) is the largest source of atmospheric particles by mass, with a global emission flux ranging from 3-30 Pg per year,³ 98% of which is attributed to supermicron particles.⁴ SSA is produced when breaking waves entrain air bubbles beneath the ocean surface, which rise to the surface and burst. This process produces two types of

1
2
3 droplets: film drops from the bursting of the bubble cap and jet drops from the collapse of the
4 bubble cavity.^{3,5} Spume droplets can also be formed from the direct action of wind on wave
5 crests; however, these large droplets (up to millimeters in diameter) are rapidly removed from
6 the atmosphere via gravitational deposition.³ Measurements of authentic marine aerosols
7 have been traditionally limited to studies performed on research cruises or at remote field
8 stations.^{6,7} More recently, usage of ocean-atmosphere simulators such as wave channels and
9 Marine Aerosol Reference Tanks (MARTs) have enabled laboratory studies to simulate the
10 complexity of the marine environment under controlled conditions.⁸⁻¹³ These experimental
11 systems use breaking waves, plunging waterfalls, or plunging jets to produce bubble plumes
12 with the correct size and surface residence time to match bubble distributions in the real
13 ocean.^{14,15} Subsequent rupturing of these bubbles at the air-sea interface produces SSA that
14 closely resemble the size distribution of SSA observed in the marine environment.
15
16

17
18
19
20
21
22
23
24 These ocean-atmosphere simulators have been compared with other laboratory SSA
25 production devices such as fritted bubblers and shown to have several key advantages.^{9,10,16}
26 While simple in design and application, fritted bubblers tend to produce less representative
27 aerosol size distributions, resulting in physiochemical discrepancies in morphology and
28 composition.¹⁶ The use of ocean-atmosphere simulators to generate realistic marine aerosols
29 has led to a variety of new insights into marine aerosol chemistry and production.¹⁷ This
30 includes the production of marine ice nucleating particles (INPs)¹⁸; the aerosolization of
31 marine microorganisms¹⁹; biochemical control of SSA composition²⁰; biogenic volatile gas
32 production²¹; physical and chemical heterogeneity of SSA^{22,23}; and SSA surface reactivity
33 and gas uptake.^{24,25} The further use of these simulators to disentangle the wide range of
34 processes that occur in the marine environment is being advanced by improvements in their
35 construction and understanding the factors which are relevant for ideal operation.
36
37
38
39
40
41
42
43

44 While many ocean-atmosphere studies have focused solely on the composition and
45 properties of freshly emitted nascent SSA (nSSA), atmospheric aging processes can
46
47
48
49
50
51
52
53

1
2
3 transform SSA through reactions with trace gases, oxidants, and sunlight. For example,
4 heterogenous reactions of SSA with HNO₃ results in the displacement of HCl, forming
5 NaNO₃.²⁵ In addition, HNO₃ reacts with the basic sites present within biologically-derived
6 organic molecules, such as lipopolysaccharides.^{26,27} In addition to SSA, the oceans are a
7 source of secondary marine aerosol (SMA), which is formed from the reactions of VOCs
8 emitted from seawater. SMA can either form as new particles via nucleation or it can
9 condense onto existing particles in the marine atmosphere, such as SSA, changing their size
10 and chemical composition.⁷ However, in field studies, it is extremely difficult to constrain the
11 biological and chemical processes which lead to SMA formation and control its properties.
12 Recently, oxidation flow reactors (OFRs) have been used to simulate both the heterogeneous
13 oxidation of SSA and the formation of SMA in laboratory studies of marine mesocosms.²⁸⁻³⁰
14
15
16
17
18
19
20
21
22
23

24 Here we detail the features and usage of a newly constructed wave channel located at the
25 Scripps Institution of Oceanography, focusing on performance and results from a two-month
26 experimental campaign which focused on the production and measurement of marine
27 aerosols. The Sea Spray Chemistry and Particle Evolution (SeaSCAPE) experiment was
28 designed to study marine chemistry, microbiology, VOCs, and aerosols across the ocean-
29 atmosphere interface, under clean, isolated conditions. To enable this, the wave channel was
30 modified to optimize the production and collection of SSA. In contrast to previous wave
31 channel experiments,^{8,20} the SeaSCAPE experiment sought to probe the influence of
32 atmospheric aging on the composition of marine aerosols. To this end, an ancillary sampling
33 device was constructed to facilitate the study of marine gases and secondary aerosol
34 formation from the seawater in the wave channel with minimal background contamination.
35 Characterization experiments informed various modifications to wave channel construction
36 and insights into best practices for operation, while also giving context for future analyses of
37 data collected using this platform. We further outline the scope and scale of the SeaSCAPE
38
39
40
41
42
43
44
45
46
47
48
49
50
51
52
53

1
2
3 experiment, including selected results that demonstrate the types of new discoveries enabled
4 by the mesocosm experiments discussed herein, with an emphasis on the incorporation of
5 atmospheric oxidation processes.
6
7

8 **2. Methods and Materials**

10 **2.1 Description of Wave Channel**

12
13 The Scripps Institution of Oceanography (SIO) wave channel is a 33 m x 0.5 m x 0.8 m
14 (L x W x H) channel located inside the Hydraulics Laboratory. The wave channel is
15 constructed of a series of 2 m long glass panels supported by a steel scaffold. When filled to a
16 depth of 0.56 m with seawater, it holds a total water volume of 11,800 L (Figure 1). Waves
17 are generated by a paddle with a surface area of 0.96 m², powered by an electromagnetically
18 driven linear motor (H2W Technologies). This design has key advantages over previously
19 used hydraulically driven motors, mainly oil-free bearings and extended operation time. The
20 paddle was operated at 0.3 Hz with a stroke length of 73 cm, which generates waves that
21 break just beyond a submerged fiberglass ramp which functions as an artificial “beach”
22 located midway down the channel (Figure 1, Location 5). This beach (2.4 m in length) starts
23 from the bottom of the flume channel and is positioned at an angle of approximately 16°
24 relative to the bottom of the channel and sits ~5 cm below the quiescent water surface. Each
25 breaking wave generates a plume of entrained bubbles with a similar size distribution and
26 residence time as those in the ocean.^{8,20} A second beach, located at the downstream end of the
27 channel (Figure 1, Location 10), serves to dissipate residual wave energy and prevent
28 disruption of wave breaking at the primary beach. The top of the channel is sealed from the
29 paddle tank to a distance 20.6 m downstream with acrylic lids, backed by marine-grade
30 plywood for support. (Figure 1c). Adhesive backed foam strips were used to create a seal
31 between the lids and the top of the wave channel, and then secured with vinyl-backed fabric
32 tape. A PTFE sheet was suspended vertically from the last lid section to the water surface to
33
34
35
36
37
38
39
40
41
42
43
44
45
46
47
48
49
50
51
52
53

1
2
3 reduce backflow of room air into the channel (Figure 1, Location 7). In addition, the open
4 section at the end of the wave channel was covered with lightweight polyethylene film to
5 prevent dust and debris from settling into the channel.
6
7

8 Sampling ports for aerosol and gas measurements of the channel headspace were
9 positioned at three locations throughout the wave channel (Figure 1, Locations 4, 6a, 6b). The
10 sampling ports consist of a stainless-steel bulkhead with a steel sampling tube which extend
11 0-10 cm below the lids into the headspace. An upstream sampling port located before the
12 wave break was used to monitor background particle and gas concentrations (Figure 1,
13 Location 4). The sampling ports downstream from the wave break were used for
14 measurements of SSA and VOCs (Figure 1, Locations 6a, 6b). The two sampling locations
15 were located 1.5 m apart to accommodate the large number of sampling devices, which were
16 positioned on top of the wave channel.
17
18
19
20
21
22
23

24 The paddle assembly, including motors, is enclosed within a tent made of flexible PTFE
25 film (TEKFILM, FEP2000E, 0.127 mm in thickness) to seal the system and prevent
26 contamination from the room air, while accommodating pressure fluctuations caused by the
27 reciprocating paddle. The box-shaped tent, which measures 244 cm length x 117 cm height x
28 80 cm depth, was fabricated with double heat-sealed edges and suspended in a stainless-steel
29 frame over the paddle (Figure 1, Location 2). The seam between the tent and the wave
30 channel metal body was sealed using polyester tape (3M 8403, 5 cm diameter). Particle-free
31 air was delivered to the wave channel from the top of the tent (Figure 1, Location 3) using a
32 custom air handling system made with galvanized steel duct pipes and stainless-steel
33 connectors to the PTFE tent and the channel. Ambient air pulled in using a custom fan-blade
34 powered by an induction motor (Marathon Electric 5THW8) was filtered through a four-stage
35 filter system (Hydrosil International), consisting of a pre-filter, activated charcoal pellets,
36 potassium permanganate (KMnO_4), and a HEPA filter. The scrubbed air was then directed
37 into the wave channel headspace. The charcoal pellets served to reduce background VOC
38
39
40
41
42
43
44
45
46
47
48
49
50
51
52
53

1
2
3 concentrations and the potassium permanganate served to remove acidic gases and other air
4 pollutants. A condensation particle counter (CPC) positioned upstream of the wave break
5 (Figure 1, Location 4) was used to continuously monitor background particle counts in the
6 headspace, indicating breakthrough from the filter system as well as leaks in the paddle tent.
7 Headspace concentrations of NO_x , SO_2 , and O_3 , as well as air velocity, temperature, and
8 relative humidity were also semi-continuously monitored from the same upstream sampling
9 location (see Section 2.5.1).

10
11
12
13
14
15 The wave channel was equipped with fluorescent lights to provide the light flux necessary
16 for photosynthetic organisms to grow within the seawater. Four light fixtures, two on either
17 side, were attached to the outside of each 2 m glass panel of the channel below the water
18 surface. Each fixture was equipped with two 120 cm fluorescent bulbs (Spectra 5700K F32-
19 T8, Full Spectrum Solutions, Inc), giving a total of 8 bulbs per panel. The lights extended the
20 full length of the channel, except for the paddle tank at the front of the channel and the end
21 tank, which are constructed of stainless steel and thus not transparent to light. The flux of
22 photosynthetically active radiation (PAR) in the channel was measured to be $\sim 80 \mu\text{E}/\text{m}^2\text{s}$ in
23 the center of the channel, approximately ~ 30 cm below the water surface (Apogee
24 Instruments, MQ-200). While this is significantly lower than typical daytime PAR levels,
25 which often exceed $1,000 \mu\text{E}/\text{m}^2\text{s}$ on clear days,³¹ it is comparable to PAR levels reported in
26 other studies for the purpose of growing marine phytoplankton.³² To approximate day/night
27 light cycles, the lights were operated on a timer which turned on for 14 hours during the
28 daytime and off for 10 hours at nighttime.

2.2 Wave Channel Characterization Experiments

29
30
31
32
33
34
35
36
37
38
39
40
41
42 Control experiments for characterizing the wave channel can be divided into two main
43 types: 1) obtaining minimum background aerosol levels and 2) optimizing the sampling
44
45
46
47
48
49
50
51
52
53

1
2
3 location and depth into the channel headspace. For the control experiments, the wave channel
4 was filled with sand-filtered coastal seawater. This seawater is continually pumped from
5 Ellen Browning Scripps Memorial Pier (Scripps Pier, 32-52'00" N, 117-15'21" W), filtered,
6 and circulated directly into the research buildings at SIO, including the wave channel. As
7 sand-filtration removes most of the large biological species ($>1-2 \mu\text{m}$) and results in
8 microbiology that differs significantly from the seawater used in mesocosm experiments, this
9 seawater was only used for wave channel characterization and testing.
10
11
12
13
14
15
16

17 **2.2.1 Background particle concentrations**

18
19 Total particle counts in the wave channel were measured before and after the wave break
20 with condensation particle counters (Magic CPC, Aerosol Devices Inc). The purpose of the
21 upstream CPC was to detect ambient particle leaks in the paddle tent and the air handling
22 system described in Section 2.1. Counts were typically very low ($\sim 3 \text{ \#/cm}^3$). The downstream
23 CPC measured the total number of particles after the breaking waves. Thus, we assume that
24 the difference between upstream and downstream particle counts is the total number
25 concentration of SSA generated by the breaking wave. During most of the study, the
26 upstream counts were negligible, thus during these periods, we assumed that all the particles
27 measured downstream were SSA generated by wave breaking.
28
29
30
31
32
33
34
35
36

37 **2.2.2 Sampling location optimization**

38
39 Aerosol size distributions of nSSA were measured using an Aerodynamic Particle Sizer
40 (APS 3321, TSI Inc) and a Scanning Mobility Particle Sizer (SMPS 3938, TSI Inc) equipped
41 with an X-ray neutralizer (Model 3088, TSI Inc) at various locations downwind of the wave
42 break (5 locations, 60 cm intervals) at 0-10 cm below the channel lid. The induction motor
43 was tuned between 1250 and 2500 rotations per minute (RPM) to vary the airflow and
44
45
46
47
48
49
50
51
52
53

1
2
3 determine the response of the total particle number concentration. Particles were dried prior
4 to measurement with a silica diffusion dryer. The electrical mobility diameters (d_m) measured
5 by the SMPS are assumed to be the same as the physical diameter (d_p). The aerodynamic
6 diameters (d_a) measured by the APS were converted to physical diameter using the effective
7 density of sea spray aerosol ($\rho_{\text{eff}} = 1.8 \text{ g}\cdot\text{cm}^{-3}$).⁹
8
9
10
11
12

13 **2.2.3 Wave channel headspace velocity**

14
15
16 Measurements of the wave channel air velocity were obtained during paddle operation by
17 injecting 50 μL of 45 mM dimethyl sulfide (DMS) in methanol into the wave channel
18 headspace at the upstream sampling port. As DMS was carried along the length of the wave
19 channel by the headspace flow, a home-built chemical ionization time of flight mass
20 spectrometer (CI-ToF-MS) drew headspace at 2 slpm from the first downstream sampling
21 port (Figure 1, Location 6a). The operation of the CI-ToF-MS instrument is described in
22 detail below (Section 2.6.2).
23
24
25
26
27
28

29 **2.3 SeaSCAPE Bloom Initiation**

30 **2.3.1 Wave Channel Cleaning Procedures**

31
32
33
34 The wave channel was cleaned and sanitized prior to all experiments and induced bloom
35 measurements. The channel was first filled and flushed with fresh water to remove any large
36 debris, then the inside walls were sprayed with a 3% acetic acid/water mixture. A
37 combination of soft sponges and brushes were used to manually remove any film or debris
38 from the inner walls. Once completed, the channel was flushed with fresh water to remove all
39 of the cleaning solution. As a final rinse, the channel was filled with sand-filtered seawater,
40 then drained.
41
42
43
44
45
46
47
48
49
50
51
52
53

2.3.2 Water Collection

Seawater was collected from the Scripps Pier. The water is pumped up from the end of the pier and travels through a gravity flume on the south side of the pier to the pier entrance. During the pumping process, the seawater passed through a rough aluminum screen to collect large marine detritus such as seaweed. A submersible pump (Grundfos UNILIFT AP12.40.04.A1) was placed into the gravity flume, and water was pumped through a hose into 1,135 L plastic tanks and transported to the wave channel by truck immediately after filling at the Scripps Pier. The seawater was further filtered to remove large particulates and zooplankton using an acid-cleaned 50- μm Nitex nylon mesh (Flystuff; Cat # 57-106) and pumped into the wave channel. During Blooms 1 and 2, the Nitex mesh was attached directly to the outlet submersible pump, which inadvertently created shear forces which damaged some of the more delicate microorganisms in the seawater. To improve the seawater collection procedure, a gravity filtration system was used during Bloom 3. Briefly, a stainless-steel frame was built to fit over the top of the wave channel, to which a sheet of Nitex mesh with a surface area of $\sim 0.5 \text{ m}^2$ was affixed. Seawater was poured over the frame, allowing it to gently filter through the mesh.

2.3.3 Bloom Initiation

Algae growth media and sodium metasilicate were added to the seawater at the beginning of each bloom cycle to promote phytoplankton growth.³³ The dates and concentrations of the nutrient additions are summarized in Table 1. The growth media was added at two locations: the upstream sampling ports (Figure 1, Location 4) and after the end of the lid sections (Figure 1, Location 9). Both the growth media and silicates were dissolved into several liters of milliQ H_2O , then slowly added dropwise to the channel using a sterilized separatory funnel or polycarbonate carboy equipped with a spigot over the course of several

1
2
3 hours. This slow nutrient addition allows the growth media to mix with the seawater in the
4 channel and prevents compounds from precipitating out of solution due to the high salinity.
5

6
7 During the third bloom cycle, a separate phytoplankton bloom was grown in a 1,135 L
8 cylindrical plastic tank outside of the hydraulics laboratory (Table 1). The purpose of this was
9 to inoculate the wave channel with healthy phytoplankton biomass grown under natural
10 sunlight to promote a larger bloom. Seawater was collected from Scripps Pier and filtered
11 using 50- μm Nitex mesh, then it was transferred to the 1,135 L outdoor tank, covered with
12 wire mesh to keep out debris, and placed in partial shade. To stimulate the growth of a
13 phytoplankton bloom, *f/2* growth media and sodium metasilicate were added immediately
14 and the seawater was bubbled gently to oxygenate. Once the outdoor tank reached the
15 exponential growth phase as indicated by *in situ* fluorescence measurements (AquaFluor,
16 Turner Designs), 1,135 L of water were drained from the wave channel, and the contents of
17 the tank were added to the wave channel. Water was transferred gently using sanitized
18 buckets to avoid damaging the phytoplankton during the transfer. Additional nutrients were
19 added to the wave channel immediately following the outdoor tank addition to bring the total
20 concentration of growth media and silicates up to *f/2* in the wave channel.
21
22
23
24
25
26
27
28
29
30
31

32 **2.4 Isolated Sampling Vessel and OFR Experiments**

33 **2.4.1 Description of Isolated Sampling Vessel**

34
35 Due to challenges associated with removing all trace gases from both the ambient air
36 brought in via the air handler and off-gassing from wave channel materials, an isolated
37 headspace was used to sample VOCs produced from seawater (see Section 2.6). The isolated
38 sampling vessel (ISV) was constructed from a single cylindrical tube of borosilicate glass
39 (Greatglas, Delaware U.S.A.) that was capped on both ends. The dimensions of the glass tube
40 were as follows: 400 mm outer diameter, 6 mm wall thickness, 74 cm long, resulting in a
41
42
43
44
45
46
47
48
49
50
51
52
53

1
2
3 total volume of 87 L and a water volume of 44 L, when filled halfway with seawater. An
4 annotated schematic of the ISV can be found in Figure S1. Each end of the ISV was sealed by
5 a PTFE disk, thickness 1.6 mm, braced against the face of the cylinder by a 9.5 mm acrylic
6 disk and backed by an aluminum frame. Six 6.4 mm stainless steel Swagelok bulkhead ports
7 in the headspace partition were used for the zero air inlet and gas sampling outlets (located on
8 opposite ends), with one 13 mm bulkhead to continuously pump seawater and a 25 mm
9 bulkhead drain port located 13 mm above the center of a PTFE sealing plate opposite of the
10 filling bulkhead.
11
12
13
14
15
16

17 Seawater was delivered to the ISV via a plunging stream located opposite the sampling
18 ports. The seawater was circulated using a peristaltic pump equipped with Tygon tubing,
19 which withdrew water from the wave channel, ~0.5 m beneath the water surface. In order to
20 maintain a consistent flow rates and prevent leaks, the tubing within the peristaltic pump was
21 replaced every 3 days. ISV water drained back into the channel through 25 mm tubing
22 attached to the large central port opposite the plunging jet, with the end of the return flow
23 tubing submerged beneath the water level. Zero air flow rate through ISV headspace varied
24 from 8-10 standard liters per minute (slpm), leading to an average air residence time of 5
25 minutes. The water flow rate was fixed at 1.5 slpm, leading to a water residence time of 29
26 minutes. The ISV was lit by two fluorescent light fixtures, which extended the length of the
27 vessel on either side. These lights were identical to those used on the wave channel and were
28 operated on the same diurnal pattern, for the purpose of maintaining the same light flux in the
29 ISV during daytime hours.
30
31
32
33
34
35
36
37
38
39
40

41 **2.4.2 OFR Operation**

42

43 To study the effect of atmospheric aging processes on marine aerosols, potential aerosol
44 mass oxidation flow reactors (PAM-OFR, Aerodyne Inc) were used to simulate both the
45
46
47
48
49
50
51
52
53

1
2
3 heterogeneous oxidation of primary sea spray aerosol and the formation of secondary marine
4 aerosol from the oxidation of VOCs. The PAM-OFR uses UV lamps to produce high
5 concentrations of OH radical, simulating atmospheric aging from a fraction of a day to
6 weeks, with a residence time of 1-3 minutes.^{34,35} Two OFRs (OFR1 and OFR2) sampled from
7 the wave channel headspace (Figure 1, Location 6a), with the goal of producing
8 heterogeneously aged SSA (hetSSA), although SMA is also produced from the oxidation of
9 VOCs present in the wave channel headspace. Figure S2 shows a schematic of the different
10 OFR sampling lines utilized during SeaSCAPE. Briefly, OFR1 was utilized for continuous,
11 online measurements of hetSSA chemical composition, size distributions, and hygroscopicity.
12 In contrast, OFR2 was utilized for a combination of online and offline measurements
13 including aerosol chemical composition, phase and morphology, and INP characteristics. A
14 third OFR (OFR3) sampled from the ISV (Figure 1, Location 8), for the purpose of producing
15 SMA under clean conditions. A full inventory of aerosol measurements conducted using the
16 OFRs can be found in Tables 2 and 3.

17
18 All OFRs were operated in OFR185 mode, meaning the UV lamps produce light with
19 wavelengths of both 185 nm and 254 nm. The OH exposure at each lamp intensity was
20 determined by introducing carbon monoxide to the OFR and measuring the drop in CO
21 concentration due to oxidation using a CO analyzer (APMA-370, Horiba Ltd). The OH
22 exposure is determined using the rate coefficient of CO + OH ($k_{\text{OH} + \text{CO}, 298\text{K}} = 1.5 \times 10^{-13} \text{ cm}^3$
23 $\text{molec}^{-1} \text{ s}^{-1}$), assuming pseudo-first order kinetics.³⁶ The OH exposure can be converted to
24 “days of equivalent aging” using typical tropospheric OH concentrations ($[\text{OH}] = 1.0 \times 10^6$
25 $\text{molec} \cdot \text{cm}^{-3}$).³⁷ O₃ concentrations were monitored downstream of each of the OFRs using an
26 O₃ analyzer (Model 202 and Model 106-L, 2B Technologies). Before aerosol measurements,
27 the sample air was passed through a denuder to remove O₃ (Carulite-200, obtained from
28 Ozone Solutions).

2.5 SeaSCAPE – Aerosol Measurements

A large suite of aerosol measurements was conducted during the SeaSCAPE experiment to study the properties of nSSA, hetSSA, and SMA. These include measurements of the size distributions, chemical composition, INP characteristics, CCN activity and water uptake, and phase state and morphology, among other properties. All measurements conducted during the campaign are summarized in Tables 2 and 3.

2.5.1 Aerosol Number and Size Distributions

Total particle counts in the wave channel were measured before and after the wave break with condensation particle counters. The aerosol size distributions of nSSA after the wave break were measured using the APS and SMPS as described in the control experiment. Size distributions from OFR1 and OFR2, which includes both hetSSA and SMA, were measured using a Scanning Electrical Mobility Spectrometer (SEMS, Brechtel Manufacturing, Inc) and an APS (3321, TSI Inc). SMA size distributions from OFR3 were measured using an SMPS (Model 3938, TSI Inc) equipped with a Nano DMA (DMA 3085, TSI Inc) and a soft X-ray Neutralizer (Model 3088, TSI Inc). The SMPS and APS systems were factory calibrated prior to the SeaSCAPE campaign. During the study, polystyrene latex spheres (PSLs) were used to verify the sizing instrument performance.

2.5.2 Single Particle Atomic Force Microscopy (AFM) Measurements

Nascent and heterogeneously aged sea spray aerosols were collected for AFM measurements of aerosol phase and morphology throughout SeaSCAPE. A selected analysis was conducted of particles collected on 8/3/19, which corresponded to the peak of the phytoplankton growth during Bloom 3. The nSSA were deposited onto hydrophobically treated silicon substrates (Ted Pella, Inc.) using a micro-orifice uniform deposit impactor

1
2
3 (MOUDI, MSP, Inc., model 110, flow rate of 30 lpm) at ca. 80% RH (i.e. wet deposition).³⁸
4
5 The hetSSA were deposited onto the hydrophobically treated silicon substrates using a
6
7 separate MOUDI (MSP, Inc., model 125R, flow rate of 10 lpm) at ca. 20% RH (i.e. dry
8
9 deposition).^{38,39} MOUDI stages 6, 7 and 8 were used, which corresponds to an aerosol
10
11 aerodynamic diameter 50% cut off range of 0.18-1.0 μm . The hetSSA were generated using
12
13 OFR2, with a UV lamp voltage of 2.0 V which corresponds to approximately 4-5 days of
14
15 photochemical aging in the atmosphere. The substrate-deposited nascent and hetSSA samples
16
17 were stored in clean Petri dishes and kept inside a laminar flow hood (NuAire, Inc., NU-425-
18
19 400) at ambient temperature (20–25°C) and pressure.

20
21 AFM height images of individual nascent and hetSSA particles were recorded using the
22
23 molecular force probe 3D AFM (Asylum Research, Santa Barbara, CA), at ambient
24
25 temperature (20–25°C) and pressure. Silicon nitride AFM tips (MikroMasch, Model NSC35,
26
27 tip radius of curvature ~ 10 nm) were used to image individual particles. A custom-made
28
29 humidity cell was used to control the RH at 50% for all imaging; the elevated RH was used
30
31 due to expected lowering of the viscosity for the organic components relative to inorganic
32
33 that facilitates differentiation of their spatial distribution using AFM.³⁸ AC mode (intermittent
34
35 contact or tapping mode) AFM was used to image individual particles and determine their
36
37 morphology. A total of 50 individual particles were characterized for each sample type.

38 39 40 **2.5.3 Aerosol Mass Spectrometry (AMS)**

41
42 The chemical composition of submicron non-refractory aerosol was determined by high
43
44 resolution time-of-flight aerosol mass spectrometry (HR-TOF-AMS; Aerodyne, Inc.).⁴⁰ A
45
46 collection efficiency of $CE = 0.65$ was applied to the data. The AMS was operated in V-mode
47
48 with standard MS mode (5s open, 5s closed) and PTOF (10s) with typically 5-min sampling
49
50 averages.
51
52
53

2.6 SeaSCAPE – Gas-phase Measurements

In addition to the gas-phase measurements discussed below, Table 4 details the full inventory of gas-phase measurements conducted during SeaSCAPE to assess questions regarding VOCs produced from seawater and anthropogenic contaminants.

2.6.1 Trace Inorganic Gases

The concentrations of trace gases were monitored at several locations: the air handling system, room air, and the wave channel headspace, upstream of the wave break. A custom-fabricated solenoid valve switching array was used to automatically switch between the different air sampling lines. The concentrations of the oxides of nitrogen (NO_x) were continuously monitored using a Model 42C NO-NO₂-NO_x analyzer (Thermo Electron Corporation). Ozone concentrations were measured using a UV photometric based O₃ analyzer (Model 49C, Thermo Electron Corporation). The analyzer was calibrated using an ozone calibration source (Model 306, 2B Technologies). Sulfur dioxide concentrations were measured using a pulsed fluorescence SO₂ analyzer (Model 43iQ Trace Level SO₂ Analyzer, Thermo Electron Corporation).

2.6.2 Chemical Ionization Time of Flight Mass Spectrometry

A home-built CI-ToF-MS using benzene cluster cation chemistry, previously described by others,^{41,42} was utilized to determine the headspace flow rate of the wave channel. Briefly, ~300 ppm benzene vapor was generated by passing 10 standard cubic centimeters per second (sccm) of N₂ over a cylinder of liquid benzene and diluted to concentration with added N₂.^{42,43} Benzene vapor was passed through a 20mCi Po-210 α -source to generate benzene cluster cation reagent ions, and further drawn through an inline critical orifice at 1.8 slpm into the ion-molecule region (IMR) of the CI-ToF-MS. Sample analyte was similarly drawn into

1
2
3 the IMR at the same flow rate as analyte. The IMR pressure was maintained at 60 Torr and
4 60 V for all analyses. Analyte ions generated through charge transfer and ligand switching
5 reactions with benzene cluster cations were focused by a radio frequency ion funnel, and
6 subsequently transferred by an RF-only quadrupole into an orthogonal-extraction time of
7 flight analyzer (Tofwerk). Co-summed mass spectra from 5-500 m/z were obtained at 1 Hz,
8 with generated data analyzed using the Tofware plugin for Igor Pro 7 software.
9
10
11
12
13
14

15 **2.6.3 Proton Transfer Reaction Mass Spectrometry**

16

17 A Vocus proton transfer reaction time-of-flight mass spectrometer (PTR-ToF-MS)
18 (TOFWERK, Aerodyne Inc.) measured headspace gas-phase VOCs.⁴⁴ The focusing ion-
19 molecule reactor was operated at high reduced field strength ($E/N = 143$ Td). It was held at a
20 pressure of 1.5 mbar, electric field of 41.5 V cm^{-1} , and temperature of $100 \text{ }^\circ\text{C}$. The big
21 segmented quadrupole voltage was 275 V, reducing the transmission of low mass ($<35 \text{ m/Q}$)
22 ions. The PTR-ToF-MS mass spectra were saved at 1 Hz time resolution. The headspace of
23 the ISV was sampled at 100 sccm through a roughly 2.5 m, 6.35 mm O.D. PFA tube. The air
24 handling system and wave channel headspace were pulled down a 9.525 mm O.D. PFA tube
25 approximately ~ 15 m at a flow rate of 8 slpm. The PTR-ToF-MS subsampled 100 sccm of
26 this flow. Room air was sampled intermittently approximately 8 times throughout the day.
27 Instrument background signals were determined about 8 times daily by overflowing the PTR-
28 ToF-MS inlet with zero air from the zero-air generator (Sabio 1001) that provided air to the
29 ISV headspace. Daily average background signals were used for background correction. Peak
30 fitting and integration were completed in Tofware 3.1.2.
31
32
33
34
35
36
37
38
39
40
41
42
43
44
45
46
47
48
49
50
51
52
53

2.6.4 Offline Atmospheric Pressure Chemical Ionization for Irradiation Experiments

Photo-initiated VOC production was measured using a high-resolution Orbitrap Elite (Thermo Fisher Scientific) mass spectrometer equipped with a modified gas-phase atmospheric pressure chemical ionization (APCI) source. Seawater samples collected during the SeaSCAPE campaign were irradiated using an LCS-100 solar simulator (94011A, Oriel), adapted from the approach used by Roveretto et al.⁴⁵ Data were collected solely in positive mode, where needle voltage was set to 4 kV, needle current at 5 mA, and vaporizer temperature at 150 °C. Sheath and auxiliary flow were set to zero. An air mass optical filter (AM 1.5G, Newport Inc.) and a water filter were used to simulate the solar spectrum and block infrared radiation, respectively. From the wave channel, 200 mL of surface water was collected and transferred into a 350 mL jacketed custom glass tube (Ace Glass Inc.) with a quartz window on each end. The surface area of the water sample in the tube was approximately 77 cm². With a headspace of 150 mL, pure nitrogen gas was used as a carrier at a rate of 200 sccm. Temperature was regulated and measured constantly to ensure minimal thermal variation ($\pm 1^\circ\text{C}$) during the experiment. The collected water settled for 2 hours before being irradiated to allow a stable surface layer to form. To verify whether the immediate spike in signal was abiotic or biotic in nature when under lighted conditions, a separate experiment using the same water, but filtered with a 0.2 μm GTTP filter (MilliporeSigma) to remove most biological material.

2.6.5 Thermal Desorption Two-Dimensional Gas Chromatography

VOCs from the ISV and from the offline irradiation experiments were collected on triple bed sorbent tubes (Tenax TA, Carbograph 1, Carboxen 1003, CAMSCO). Samples were collected at 100 sccm for 20 minutes from the ISV headspace and 200 sccm for 10 minutes

1
2
3 from the offline irradiation experimental setup. Samples were frozen immediately after
4 collection and were analyzed offline by Thermal Desorption (Gerstel TD 3.5) two-
5 dimensional Gas Chromatography (Agilent 7980 A), modulated by two stage thermal
6 modulation (Zoex), coupled with variable energy Electron Ionization Time of Flight Mass
7 Spectrometry (Markes BenchToF) (TD-GCxGC-EI-ToF-MS). Data was collected at 50 Hz,
8 and ionization energies oscillated rapidly between 70 eV and 14 eV to simultaneously
9 generate two sets of chromatograms for each sample. The hard ionization (70 eV EI)
10 significantly fragments analytes to produce structure-specific fragmentation patterns, whereas
11 the soft ionization (14 eV EI) preserves the parent ion for comparison to chemical ionization
12 techniques. Column materials and thermal methods are as described in Hatch et al.⁴⁶
13
14
15
16
17
18
19
20
21
22

23 **2.7 SeaSCAPE – Water Measurements**

24
25
26 Seawater measurements sought to characterize both the biotic and abiotic drivers of
27 marine particles and gases, including nutrient availability, organic chemical composition,
28 biological speciation, biological productivity, dissolved gas turnover and other important
29 factors. Table 5 lists the seawater and sea surface microlayer (SSML) measurements made
30 through the duration of SeaSCAPE.
31
32
33
34
35

36 **2.7.1 Bulk Seawater Sampling**

37
38
39 Bulk seawater was sampled daily from the end of the wave channel (Figure 1, Location 9)
40 for the following analyses: dissolved organic carbon (DOC); inorganic nutrients; extracted
41 chl-a; bacterial and viral abundances; phytoplankton identification; enzyme measurements;
42 16S and 18S rDNA amplicon sequencing; and tandem mass spectrometry (MS/MS) based
43 metabolomics. Seawater was collected using a ~2 m long siphon constructed from Teflon
44
45
46
47
48
49
50
51
52
53

1
2
3 tubing. Nalgene carboys were used to transport and dispense the collected seawater for
4 analysis. Both the siphon and the carboys were rinsed with methanol, 70% ethanol, 0.1 M
5 HCl solution, and ultra-purified water prior to water collection. The siphon was inserted
6 approximately 20 cm below the surface of the water. Approximately 16 L of bulk seawater
7 were collected daily around 09:30 PST. The volume of collected seawater was replenished by
8 adding a corresponding volume of Milli-Q (Millipore) water ($<18 \mu\Omega$) every other day to
9 maintain the water level in the flume without introducing any microbiological contaminants.
10
11
12
13
14
15
16

17 **2.7.2 Sea Surface Microlayer Sampling**

18

19 Sea surface microlayer (SSML) samples were collected from the same location as the
20 bulk seawater (Figure 1, Location 9). The collection was conducted using a glass plate, a
21 glass funnel and a Teflon scraper. During the day preceding collection of SSML samples, the
22 glass plate and funnel were cleaned of biological material using Millipore water, methanol,
23 70% ethanol, and 10% HCl. The collection glassware was placed in a combustion furnace for
24 5 hours at 500 °C to remove organic contaminants. The glass plate with a handle was lowered
25 carefully into the wave channel at a rate of 5-6 cm s⁻¹ and withdrawn at the same rate. This
26 withdrawal rate corresponds to an estimated sampled SSML thickness of around 50 μm.^{47,48}
27 After removal from the wave channel, the glass plate was suspended for 20 seconds to allow
28 any bulk seawater to drain off the plate and back into the channel, ensuring that the majority
29 of remaining material was SSML. The remaining liquid was scraped from the glass plate into
30 a collection vessel using a Teflon scraper. This process was repeated until approximately 200
31 mL of sample was collected.
32
33
34
35
36
37
38
39
40
41
42
43
44
45
46
47
48
49
50
51
52
53

2.7.3 DOM Extraction and Compositional Analysis

Dissolved organic matter (DOM) was extracted from bulk seawater samples collected from the wave channel (Figure 1, Location 9) using the solid phase extraction method described and characterized by Dittmar and coworkers (Dittmar 2008). At the end of Bloom 3, a large volume of about 2,000 L was extracted over the course of 72 hours using this method. A total of 1.51 ± 0.01 g of marine DOM was collected and stored at -18 °C for future analyses.

Samples of extracted DOM were analyzed by TD-GCxGC-EI-HR-ToF-MS. DOM samples were reconstituted in methanol immediately prior to analysis and injected onto quartz fiber filter segments, then doped with a custom blend of 23 deuterated internal standard compounds prior to analysis, allowing corrections for instrument condition and matrix effects across samples. Briefly, the instrument thermally desorbs samples from the filter media, then introduces them into the GC oven. The instrument employs online derivatization during thermal desorption with MSTFA (n-methyl-n-trimethylsilyl-trifluoroacetamide). Analytes are separated by volatility and then by polarity by two GC columns in sequence. Separated analytes from are ionized by 70 eV electron ionization (EI) and detected by HR-ToF-MS (Tofwerk). Methodological details follow Worton et al.⁴⁹ Six-point calibration curves of custom standard blends containing ~150 representative organic compounds were performed periodically throughout sample analysis for each sample medium class to maximize quantification accuracy.

2.7.4 Chlorophyll-a, Dissolved Oxygen, and DOC Measurements

A continuous time series of *in vivo* chl-a and dissolved oxygen was measured throughout all three wave channel experiments using an Environmental Sample Processor (ESP). The ESP was located at the back of the wave channel just before the wave-dampening beach

1
2
3 (Figure 1, Location 9). The ESP is a homemade, continuous flow system that pumps seawater
4 through tubing at a flow rate of ~1 lpm using a peristaltic pump. The seawater first passed an
5 SBE 37 MicroCAT that measures conductivity, followed by an SBE 63 optical dissolved
6 oxygen sensor before being deposited into a reservoir. In the reservoir, chl-a is quantified
7 through fluorescence measurements using a Sea Bird Scientific ECO-Triplet-BBFL2 sensor
8 at excitation/emission wavelengths of 470/695 nm. After measurement of chl-a, the seawater
9 is circulated out of the ESP and back into the wave channel.
10
11
12
13
14

15 Each morning, the ESP was rinsed by circulating Millipore water through the tubing for
16 20 minutes, and every fourth day, solutions of 0.1% bleach, 30% ethanol, and Millipore water
17 were sequentially circulated through the tubing for 20 minutes to thoroughly clean the
18 instrument. This helped prevent biological growth in the tubing and biofouling of the optics.
19 Additionally, in between each experiment, the reservoir was removed from the laser optics
20 and both were carefully wiped with 70% ethanol. Any ESP measurement periods that were
21 affected by instrument maintenance or biofouling were corrected using *in vivo* chl-a
22 measurements made by a hand-held fluorometer (AquaFluor, Turner Designs). AquaFluor
23 chl-a measurements were made every few hours from the seawater sampling section of the
24 wave channel.
25
26
27
28
29
30
31

32 To calibrate both the ESP and AquaFluor chl-a measurements, chl-a was extracted from
33 the bulk seawater and analyzed by fluorometric analysis in accordance with CALCOFI
34 methods.⁵⁰ The seawater was collected once daily from the wave channel (as described in
35 Section 2.7.1) and filtered on 25 mm Whatman GF/F filters. The filters were then submerged
36 in 8 mL of 90 % acetone for 24 hours at -20 °C to extract the chl-a. Concentrations of the
37 extracted chl-a were determined by a calibrated fluorometer (10AU, Turner Designs). The
38 extracted chl-a measurements were separately plotted against both the ESP and AquaFluor
39 data, and each plot was fitted with a least squares regression used to calibrate the ESP and
40
41
42
43
44
45
46
47
48
49
50
51
52
53

1
2
3 AquaFluor chl-a values. A continuous time series of the calibrated ESP chl-a data for all three
4 experiments is shown in Figure 2.
5

6 For DOC measurements, two 40 mL aliquots of the bulk seawater (see Section 2.7.1 for
7 details of water collection) were filtered into combusted glass vials through a Whatman GF/F
8 filter, which has a pore size of 0.7 μm .⁵¹ Functionally this implies that the DOC was
9 comprised of OC with diameters $<0.7 \mu\text{m}$. The vacuum filtration was carried out using a hand
10 pump to minimize cell lysis during filtration. The DOC samples were immediately acidified
11 to pH ~ 2 with three drops of concentrated HCl and stored in a covered box at room
12 temperature until analysis. All DOC concentration measurements were made on a Shimadzu
13 TOC-V_{CSH} catalytic combustion oxidation instrument.
14
15
16
17
18
19
20
21

22 **2.7.5 Phytoplankton Enumeration and Photography**

23
24 In order to determine the taxonomic composition of the mesocosm, two methods were
25 employed: 1) Whole seawater samples were collected and manually counted under confocal
26 microscopy; 2) A dual version of the Scripps Plankton Camera System (SPCS:
27 <https://spc.ucsd.edu>) was placed on the bottom of the wave channel to continuously image the
28 developing plankton community for *in situ* observations. The SPCS was positioned at the
29 downstream end of the channel, just in front of the dampening beach (Figure 1, Location 9).
30 For the manual counting method, 400 mL of seawater was collected from approximately 30
31 cm depth at both ends of the wave channel. Samples were taken twice per day with Teflon
32 tubing and poured gently into amber Nalgene bottles. Samples were immediately fixed with a
33 2% buffered formalin solution and stored at 6 °C to preserve samples for enumeration. From
34 these, 50 mL subsamples were then poured into a settlement chamber and allowed to settle
35 for 24 hrs. The cells were prepared for enumeration using the Utermöhl method under an
36 Olympus IX-71 inverted microscope.⁵² Samples from the settlement chamber were counted to
37
38
39
40
41
42
43
44
45
46
47
48
49
50
51
52
53

1
2
3 calculate the cell concentrations per L for each distinct species. Then, the taxa cell counts
4 were binned into functional phytoplankton types, including a microzooplankton group. These
5 bins were used to calculate the relative abundance of the functional groups over time and
6 were then compared to the *in-situ* camera data.
7
8
9

10 The *in-situ* camera enabled the research team to study the plankton community
11 undisturbed in the mesocosm, monitor the presence of delicate taxa, and observe intra- and
12 inter-species interactions. The goal of the image analysis was to target detritus, aggregates,
13 phytoplankton and zooplankton between 20-1000 μm in major axis length. For this reason,
14 only images collected by the 5x magnification system of the SPCS were considered. Over the
15 course of the 3-week experiment, nearly 1.85×10^6 images of particles were collected within
16 this size range. The system uses darkfield illumination to image free-floating particles in
17 approximately 3 μL /frame sampling volume with a resolution of 3-5 μm .⁵³ In order to train a
18 neural net to classify this large amount of data, a subset of the images was manually labelled
19 to serve as a training set.
20
21
22
23
24
25
26
27
28

29 **2.7.6 Bacteria, virus, nano-and picophytoplankton, and heterotrophic** 30 **nanoflagellates enumeration** 31 32

33 Bacteria, cyanobacteria and viruses in the seawater, SSML and nSSA were
34 enumerated with a BD FACSCanto II™ flow cytometer (FCM). Samples were prepared
35 according to established protocols.⁵⁴⁻⁵⁶ All samples were preserved with glutaraldehyde at
36 5% final concentration and stored at -80°C .⁵⁷ For heterotrophic bacteria staining, the samples
37 were diluted with Tris-EDTA buffer (pH 8), then stained with SYBR Green.⁵⁴ For virus
38 staining, water was diluted (1:50) in 1×TE buffer (pH 8) and stained with SYBR Green.⁵⁵
39 Aliquots of seawater and SSML samples were analyzed unstained for counting
40 *Cyanobacteria* ⁵⁸. SSA samples were collected into 0.7 mL 4X PGE (prepared as 4x PBS,
41
42
43
44
45
46
47
48
49
50
51
52
53

1
2
3 20% glycerol, 20 mM EDTA) buffer using a Liquid Spot Sampler (SS110A, Aerosol Devices
4 Inc), which sampled at 1.8 lpm.⁵⁹ The liquid sample was brought to 1 mL by adding 4XPGE,
5 then split into two 0.5 mL aliquots that were processed as described above for FCM counting
6 of heterotrophic bacteria and viruses. SSA blank samples were also collected via Spot
7 Sampler with a HEPA filter on the inlet and processed accordingly. The values counted in the
8 same SSA blank gates were subtracted from the SSA sample runs. For heterotrophic bacteria
9 and viruses, the samples were analyzed at medium rate ($60 \mu\text{L min}^{-1}$) with a threshold set on
10 green fluorescence. Side scatter versus green fluorescence plots were generated to identify
11 and quantify heterotrophic bacteria and viral populations.^{56,58} *Synechococcus* population were
12 identified on forward scatter versus orange fluorescence and red fluorescence. Samples for
13 nano, picophytoplankton and heterotrophic nanoflagellates were run on a BD Accuri FCM
14 following established protocols.^{60,61}
15
16
17
18
19
20
21
22
23
24
25

26 **3. Results: Characterization and Optimization of the Wave Channel**

27 **3.1 Contaminant contributions to wave channel headspace composition**

28
29
30 The concentration of trace inorganic gases (NO_x , SO_2 , CO , and O_3) were monitored in
31 the wave channel headspace, as the air handling system is not expected to fully remove these
32 gases. In the remote marine boundary layer, NO_x mixing ratios are typically less than 50
33 ppt.⁶² During the SeaSCAPE campaign, the NO_x concentration in the channel headspace was
34 significantly higher, with a mean concentration of 1.4 ppb (Table S1, Figure S3). This is
35 lower than typical ambient concentration expected in an urban area (10-100 ppb),⁶³ indicating
36 that the air handling system was able to scrub some ambient NO_x ; however, it was not able to
37 achieve levels as low as the clean marine boundary layer. Conversely, while the air handling
38 system failed to remove all of the O_3 from the headspace air, the resulting concentrations
39
40
41
42
43
44
45
46
47
48
49
50
51
52
53

1
2
3 (average $[O_3] = 16$ ppb, Table S1) were actually comparable to background concentrations
4 observed in the Atlantic boundary layer (~15-20 ppb).⁶⁴
5

6
7 Volatile organic compounds were measured in the wave channel headspace, air
8 handling system, ISV, and room air, with PTR-ToF-MS to determine whether they originate
9 from a marine biogenic source or anthropogenic contamination (Figure 3). Dimethyl sulfide
10 (DMS) and methanethiol (MeSH) were chosen as proxies for expected marine biogenic
11 VOCs in comparison to benzene and toluene which are more closely associated with
12 anthropogenic pollutants and are not expected to be produced biogenically in large quantities
13 in the marine environment.⁶⁵ Figure 3 shows that benzene and toluene were most elevated in
14 room air, the air handling system, and the wave channel headspace, but were significantly
15 diminished in the ISV. These results suggest that the primary source of benzene and toluene
16 in the wave channel was not derived from the seawater, but likely as breakthrough of the air
17 handling system. Conversely, the concentrations of DMS and MeSH in the ISV were
18 significantly elevated compared to the wave channel, due to the lower air flow rate and higher
19 relative water surface area. These results show that the ISV was effective in maintaining a
20 clean headspace that better reflects the emissions of gases present in seawater with minimal
21 anthropogenic background.
22
23
24
25
26
27
28
29
30
31
32
33

34 **3.2 Wave channel headspace velocity**

35

36
37 Given the unique aspects of the wave channel, which features a highly longitudinal
38 construction, with air introduction at one side, and a propagating water wave inside, a short
39 investigation was undertaken to determine the headspace flow velocity along the channel
40 length at a fan speed of 1500 RPM using spikes of injected DMS at the upstream port. Shown
41 in Figure 4 is the arrival of DMS spikes at the downstream sampling port (Figure 1, Location
42 6a) measured by CI-ToF-MS. Mean arrival time was 200 ± 35 seconds (N=3) with the paddle
43
44
45
46
47
48
49
50
51
52
53

1
2
3 running. Replicate experiments with the paddle stationary did not yield arrival times that
4 significantly differed. Given the distance of the upstream sampling port from the downstream
5 ports, the wave channel headspace velocity was calculated to be 4.9-7.0 cm/second. Large
6 variability in the measured headspace velocity suggests turbulent flow conditions in the wave
7 channel, which is further supported by aerosol concentrations discussed later.
8
9
10
11
12

13 **3.3 Characterization of particle backgrounds and SSA production**

14
15
16 Background particle concentrations were measured in the wave channel headspace at the
17 upstream sampling port (Figure 1, Location 4) using a CPC to determine the contribution of
18 non-marine particles from sources such as leaks in the paddle tent or breakthrough in the air
19 handling system while the waves were being generated. Setting the RPM of the induction
20 motor that supplied clean air to the wave channel to a speed less than 1500 RPM introduced
21 ambient non-marine particles into the wave channel headspace (10-50x more than fan speeds
22 greater than 1500 RPM), thus establishing a lower limit of the air handling unit. While
23 increasing the speed of the motor could increase the amount of clean air into the headspace of
24 the wave channel, doing so dilutes the total number of SSA from wave breaking. Thus, our
25 testing found that 1500 RPM was the optimal fan speed (Figure 5a, Figure S4) and this
26 setting was used for all subsequent experiments.
27
28
29
30
31
32
33
34

35 With the optimized setting of the air handling unit, these background particle
36 concentrations were generally low ($\sim 3 \text{ \#/cm}^3$), indicating that the wave channel headspace
37 was quite clean, with respect to ambient particulate contamination ($\sim 10,000 \text{ \#/cm}^3$). In
38 comparison, the average particle concentrations after the breaking wave were significantly
39 higher ($242 \pm 91 \text{ \#/cm}^3$), indicating that the vast majority ($>98\%$) of the particles sampled
40 downwind of the breaking wave were sea spray aerosols produced in the wave channel.
41
42
43
44
45
46
47
48
49
50
51
52
53

1
2
3
4
5
6
7
8
9
10
11
12
13
14
15
16
17
18
19
20
21
22
23
24
25
26
27
28
29
30
31
32
33
34
35
36
37
38
39
40
41
42
43
44
45
46
47
48
49
50
51
52
53

With the air handling unit and the background optimized, the next step was to optimize the sampling location for SSA downwind of the breaking waves. Five locations at 0 cm, 60 cm, 120 cm, 180 cm, and 240 cm downwind of the breaking wave were tested. Interestingly, the shape of the APS and SMPS size distributions do not change significantly between the different sampling locations, whereas the total particle concentrations do exhibit variability (Figure S5). Thus, the size distributions were used to calculate the total SSA number at each location. Figure 5b shows that position 4, which corresponds to 180 cm downwind of the breaking waves, had the highest SSA number concentrations. The continuous water and air flows pushed the entrained air bubbles and the generated SSA downwind of the breaking wave.^{3,8} In addition to sampling location, the sampling port (1.27 cm i.d.) depth was tested, from 0 cm to 10 cm into the headspace as measured from the lid panel. While the specific relationship between port depth and SSA number concentration varied with sampling location, at position 4, a port depth of 5 cm yielded the highest values. However, lack of clear trend in the total number concentration as a function of sampling location and depth indicates that there may be heterogeneous mixing within the wave channel headspace due to flow turbulence. In addition, factors such as wall losses and gravitational deposition of particles may have influenced the variability in particle numbers. It was observed during testing that sampling port depths of 10 cm or greater were prone to splashing by the breaking waves, resulting in water being pulled into the sampling lines. Similarly, a port depth of 0 cm (flush with the lid surface) resulted in condensation from the lids being pulled into the sampling lines. Thus, from an operational standpoint, a sampling port depth of 2-8 cm is ideal to minimize the introduction of water to the sampling lines.

4. Results from the SeaSCAPE Experiment

4.1 Biological dynamics of phytoplankton blooms

While three distinct phytoplankton bloom experiments were performed during SeaSCAPE, results from the third bloom experiment will be focused on in this manuscript due to the large amount of data taken during the full study. In addition, the most complete suite of measurements was taken during Bloom 3. The time series of seawater chl-a, heterotrophic bacteria, and dissolved organic carbon, shown in Figure 2a, provide an overview of the biological progression of Bloom 3. Chl-a time series for Blooms 1 and 2 are shown in Figure S6. No significant phytoplankton growth was observed after the first nutrient addition (chl-a $< 2 \mu\text{g/L}$, Figure 2a), possibly due to light limitation. A phytoplankton bloom was induced in an outdoor tank with natural seawater collected as before and then added to the wave channel on 8/1 (Table 1). After the addition of the outdoor-grown bloom, the phytoplankton growth continued and peaked at $25 \mu\text{g/L}$ chl-a, and then proceeded through an extended senescent phase (Figure 2a). Following the peak of the bloom, chl-a concentrations remained stable around $5 \mu\text{g/L}$, higher than the pre-bloom state, suggesting some phytoplankton growth was still occurring. Bacterial and viral dynamics (Figure 2a) followed a typical microbial succession generally observed during phytoplankton bloom.⁶⁶

The combination of *in-situ* camera and inverted microscopy, along with chlorophyll concentrations over time, confirmed a distinct natural bloom progression in Bloom 3 (Figure 6). Phytoplankton community structure was initially dominated by diatoms (composed mostly of *Skeletonema sp.* and *Cylindrotheca sp.*) with an overall relative abundance of 55% and 1.9×10^6 cells/L. The community then shifted towards an aggregation of diatoms (composed mostly of *Cylindrotheca sp.* and *Navicula sp.*) at the end of the bloom with a relative abundance of 33% and 5.0×10^5 cells/L. There was also a proliferation in microzooplankton (composed mostly of tintinnids and copepods) at the end of the bloom with

1
2
3 a relative abundance of 25% and 5.452×10^3 cells/L. Phytoplankton physiology across the
4 bloom was screened with both methods, and showed signs of pigment loss, broken frustules,
5 and increased aggregation over time.
6
7
8
9

10 **4.2 Temperature, relative humidity, dissolved gases, and DOC**

11

12 Over the course of Bloom 3, dissolved organic carbon steadily increased in concentration,
13 due to both primary production and bacterial production of DOC, which is consistent with
14 previous bloom incubation experiments.²⁰ Notably, the addition of the outdoor tank resulted
15 in a DOC increase of 100 μM compared to the background level of the first week. The
16 dissolved inorganic gases, O_2 and CO_2 , varied on a diurnal basis as the phytoplankton utilized
17 light for photosynthesis and produced O_2 as a byproduct during the daytime. During periods
18 of higher chl-a (Figure 2a), after the outdoor tank amendment, dissolved O_2 concentrations
19 were generally more elevated, except for 8/2 when the heterotrophic bacteria reached a local
20 maximum concentration. The dissolved CO_2 concentration steadily decreased with respect to
21 chl-a due to increased carbon fixation by phytoplankton. After reaching a minimum on 8/5
22 (Figure 2b), the CO_2 concentration began increasing during the senescent phase of the
23 mesocosm probably in response to increased bacterial respiration relative to carbon fixation
24 by phytoplankton.
25
26
27
28
29
30
31
32
33
34

35 The seawater temperature of the wave channel initially began at the temperature of the
36 ocean (17°C) but equilibrated quickly to the temperature of the hydraulics laboratory within
37 ~ 24 hours (Figure 2b). Daily, temperature varied $\sim 0.75^\circ\text{C day}^{-1}$ with the ambient temperature
38 of the laboratory. Longer term variation in water temperature followed changes in local
39 weather but ranged between 24.5 - 27°C for the duration of experiment after initial
40 equilibration. The air temperature and relative humidity in the wave channel headspace also
41 exhibited a strong diurnal cycle (Figure S7). The mean air temperature during the campaign
42
43
44
45
46
47
48
49
50
51
52
53

1
2
3 was $24 \pm 1^\circ\text{C}$ and the relative humidity was $86 \pm 5\%$ (Table S2). Keeping both the seawater
4 and headspace air at controlled temperatures will be one of the key improvements of future
5 setups to more accurately simulate real ocean conditions.
6
7
8
9

10 **4.3 Impact of transportation and biological activity on seawater dissolved organic** 11 **matter** 12 13

14
15 Two selected analyses of DOM are shown here to illustrate various factors which
16 influenced the seawater chemistry: the impact of 1) seawater transportation and 2)
17 phytoplankton growth on the DOM composition. In order to fill the SIO wave channel,
18 11,800 L of seawater must be collected from the ocean and transported into the laboratory
19 facility. Due to the handling of the seawater, there is concern that the process may introduce
20 anthropogenic contaminants to the water. Figure S8 is a GCxGC ion chromatogram of
21 seawater obtained from the ocean before addition to the wave channel. Notable in the
22 composition of this seawater is the vast chemical diversity of the sample, as well as a large
23 number of known anthropogenic contaminants, such personal care products and plasticizers.
24 These species are ubiquitous in the coastal zone and are unavoidable in mesocosm
25 experiments using coastal seawater.^{67,68}
26
27
28
29
30
31
32
33

34 To understand the effect of physical transport on the chemical composition of the
35 seawater during SeaSCAPE, TD-GCxGC-EI-HRTofMS was performed on DOM samples
36 from seawater gathered from the SIO pier before and after transfer to the wave channel on
37 7/23. As a comparison, we also analyzed DOM of the seawater after the addition of the
38 outdoor phytoplankton culture on 8/1 to understand the influence of biological processes on
39 DOM. Figure 7a shows a spectral comparison plot in which the ion intensity chromatogram
40 obtained after the water transfer was subtracted by the chromatogram obtained before the
41 water was transferred. Within the limits of GCxGC sensitivity, we found that few compounds
42
43
44
45
46
47
48
49
50
51
52
53

1
2
3 were introduced by the transfer process, with less than 4% of the ion current in the post
4 transfer sample attributable to species classified as water transfer introduced contaminants
5 (Figure 7b). In contrast to the small changes made by water transfer, a much larger change
6 was measured in DOM after the addition of the outdoor phytoplankton tank to the wave
7 channel, with over 87% of the GCxGC signal introduced or significantly enhanced after the
8 perturbation (Figure 7b). This is likely due to organic material being actively produced by
9 biological activity in the seawater. Thus, we find that transportation of the seawater to the
10 wave channel has a relatively small effect on seawater composition, especially in contrast to
11 the large changes induced by phytoplankton growth.
12
13
14
15
16
17
18
19

20 **4.4 nSSA Size Distributions and Stability**

21
22
23 The shape of the nSSA size distributions is largely consistent with previous studies of
24 SSA generated by breaking waves (Figure S9).⁸ However, there was significant temporal
25 variability in the total concentration of particles observed during the experiment. A strong
26 diurnal trend was observed, with higher, more variable concentrations observed during the
27 daytime ($N_{\text{day}} = 272 \pm 92 \text{ \#/cm}^3$) and lower, yet more stable concentrations observed during
28 the nighttime ($N_{\text{night}} = 199 \pm 70 \text{ \#/cm}^3$) (Figure 8). While seawater temperature can affect the
29 flux of nSSA, the daily changes observed during the SeaSCAPE experiment were likely not
30 large enough to explain the variability in nSSA concentration.³ Typical daily water
31 temperature changes were less 1°C (Figure 2), which should correspond to a change in SSA
32 flux of only 2-4%,⁶⁹ whereas the observed change from night to day is, on average, ~37%.
33 The diurnal changes also do not appear to be linked to other changes such as the wave
34 channel lights, biological productivity, or the chemical composition of the seawater. Rather,
35 we suspect that the changes in SSA production were driven by the opening and closing of the
36 laboratory doors, which may have affected the air flow and mixing dynamics within the
37
38
39
40
41
42
43
44
45
46
47
48
49
50
51
52
53

1
2
3 channel headspace. These findings, alongside the results of the sampling port location and
4 depth testing (Figure 5b), demonstrate the turbulent mixing within the wave channel
5 headspace, resulting in variable nSSA number concentrations. Further testing and modelling
6 studies of the wave channel are necessary to fully understand these observations.
7
8
9

10 11 12 **4.5 Characteristics of hetSSA and SMA produced in the OFRs**

13
14 OFRs were used to assess the effects of atmospheric aging on gases and particles emitted
15 from the oceans. While the primary goal of the OFR1 and OFR2 experiments was to assess
16 the effects of photooxidative aging on the properties of SSA (referred to as hetSSA herein),
17 the gases present in the wave channel headspace were not removed and thus also reacted in
18 the OFRs. New particle formation was observed due to the reactions of these gases, as
19 evidenced by the appearance of a large nucleation mode in the aerosol distributions when the
20 OFRs are active (Figure 9a). The formation of SMA in OFR1 and OFR2, both as nucleated
21 particles and via condensation onto SSA, presents a significant challenge for the
22 measurement of hetSSA. Size-resolved measurements can overcome this by simply selecting
23 for particle sizes larger than the ultrafine mode ($D_p > \sim 100$ nm) and thus presumed to be
24 primary SSA particles. These larger SSA particles may contain secondary species but will
25 have also undergone heterogeneous oxidation by OH radical and ozone in the OFR.
26 Measurements of the bulk non-refractory aerosol show significant changes in chemical
27 composition due to oxidation processes in the OFR. In the bulk chemical speciation shown in
28 Figure 9, the relative increase in particulate nitrate, compared to non-refractory particulate
29 chloride, is consistent with heterogeneous reaction of $\text{HNO}_3 + \text{NaCl} \rightarrow \text{NaNO}_3 + \text{HCl}$.⁷⁰ The
30 displacement of chloride for nitrate has been previously observed in coastal sea spray
31 aerosol⁷¹ and explored in laboratory experiments.^{25,72} In our experiment, this anion
32
33
34
35
36
37
38
39
40
41
42
43
44
45
46
47
48
49
50
51
52
53

1
2
3 substitution indicates that HNO_3 is likely produced in the OFR when sampling the wave
4 channel head space air through the oxidation of NO_x to form HNO_3 .

5 6 **4.6 Evidence of abiotic volatile organic compound production from interfacial** 7 8 9 **photochemistry**

10
11 To test whether VOCs could be produced abiotically by irradiating the organic surface
12 species with sunlight, surface water from the wave channel was exposed to light from a solar
13 simulator and analyzed using a modified gas-phase APCI Orbitrap MS. Shown in Figure 10a,
14 two unique molecular signatures were significantly enhanced upon irradiation compared to
15 other measured m/z signals, as well as three others not shown here (isoprene, dimethyl
16 sulfone, and decadienal only in some days during Bloom 3). Several other species, many
17 unidentified, also increased during this time but exhibited a more gradual increase, indicating
18 a diffusion limited, and therefore most likely biogenic or non-surface related, process.^{73,74}
19 Two of these species, generated via irradiation, were annotated using tandem MS, showing
20 fragmentation patterns that indicated the presence of phenol, $\text{C}_6\text{H}_6\text{O}$, and possibly beta-
21 cyclocitral, $\text{C}_{10}\text{H}_{16}\text{O}$. The signal enhancement of these molecules immediately upon
22 irradiation (within 3 minutes), compared to the background dark signal, are shown in Figures
23 10b and 10c respectively. The fragmentation pattern of $\text{C}_{10}\text{H}_{16}\text{O}$ suggests that beta-cyclocitral
24 was the dominant species with this mass-to-charge ratio, but multiple other isobaric species
25 contributed a minor signal. Without an in-depth experiment to constrain the many variables in
26 seawater such as the microbiology, including viruses and enzymes not removed by filtration,
27 or surface tension, it is difficult to make any assumptions about the specific mechanisms
28 responsible for photo-initiated VOC production. Only recently have studies begun to explore
29 the mechanisms of interfacial VOC production at the ocean surface. Models and uncertainties
30 in field measurements point towards a significant source of abiotic compounds.^{73,75} Gas-
31 phase APCI Orbitrap MS was shown to successfully ionize a variety of molecular signatures
32
33
34
35
36
37
38
39
40
41
42
43
44
45
46
47
48
49
50
51
52
53

1
2
3 off-gassing from the seawater surface as well as detect changes when the sample was exposed
4 to solar light.
5
6

7 8 **4.7 Relative distribution of morphologies for nascent and hetSSA** 9

10 Nascent SSA displayed four unique morphologies including prism-like, core-shell,
11 rounded and aggregates, while hetSSA had two main morphologies: core-shell and rounded
12 (Figure 11a). The morphological categorization was performed qualitatively, analogous to
13 previous studies.^{23,76} Next, the relative distribution of morphologies for nSSA and hetSSA
14 samples were compared (Figure 11b). For the nSSA sample morphologies, the rounded
15 (47%) was most common, followed by the core-shell (22%), while prism-like (17%) and
16 aggregates (14%) showed similar abundancies. On the other hand, for the hetSSA sample
17 morphologies, core-shell (72%) was most common, followed by the rounded (28%)
18 morphology, while no prism-like and aggregates were observed. Overall, SSA aging results
19 in significant increase of the abundance for core-shell morphology, and concomitant
20 decreases in the other morphologies. Additionally, core-shell hetSSA particles showed a
21 thicker coating compared with similar-size nascent core-shell particles.
22
23
24
25
26
27
28
29
30
31
32

33 **5. Discussion** 34

35 **5.1 Wave channel characterization** 36

37 A key challenge in ocean-atmosphere simulation experiments is maintaining the highest
38 degree of experimental cleanliness while still capturing the complexity of the natural
39 environment. This challenge is further pressed by the massive volumes of seawater that must
40 be collected and transferred without significant perturbation of the biological assemblages
41 and chemical contamination of the water. For the headspace, large airflows are necessary to
42 offset the flow demand required by online instrumentation and filter sampling. Generating
43
44
45
46
47
48
49
50
51
52
53

1
2
3 large volumes of high purity air is a significant challenge beyond the removal of particulates.
4 Here we showed that the transfer of seawater from the ocean to the laboratory incurred little
5 contamination; however, there was significant breakthrough of anthropogenic contaminants
6 in the air handling system. The incorporation of the ISV was a critical addition that enabled
7 the measurement of secondary marine aerosol and gases by generating a clean headspace for
8 seawater VOCs to partition into. In the future, advances in economically generating high
9 volumes of particle-free, ultrapure air would be ideal to enable the measurements of
10 seawater-produced VOCs without the incorporation of secondary chambers.
11
12
13
14
15
16

17 Systematic testing of the wave channel was conducted to determine the optimal sampling
18 conditions for nascent SSA. This testing showed a clear relationship between the air flow rate
19 in the channel headspace and the measured concentrations of SSA particles, with lower air
20 speeds resulting in higher particle concentrations. However, when the effect of both sampling
21 port location and penetration depth into the channel headspace were evaluated, it was
22 apparent that the nSSA concentrations in the headspace were heterogeneous and highly
23 variable, depending on sampling locations. Further observations during the SeaSCAPE
24 experiment showed a strong diurnal trend in the nSSA concentrations, which may have been
25 caused by the opening and closing of the laboratory doors, creating a change in air pressure in
26 the building. Based on these findings, future work is needed to model the fluid dynamics in
27 the wave channel to understand the mixing and transport of aerosols and gases in the
28 headspace. Additionally, it was observed that nSSA concentrations were typically more
29 stable at night when the laboratory doors were closed, which reduced ambient air movement
30 in the facility. This suggests that future modifications could be made to the wave channel to
31 increase stability in the particle concentrations, such as replacing the open flap at the end of
32 the channel with an improved vent system to control air flow. However, despite the
33 variability in total number concentrations, the shape of the SSA size distributions remained
34 consistent throughout the experiment and agrees well with previous wave channel
35
36
37
38
39
40
41
42
43
44
45
46
47
48
49
50
51
52
53

1
2
3 experiments.⁸ This indicates that the variability in the number concentrations was driven by
4 different degrees of dilution, due to uneven mixing in the headspace, as opposed to variations
5 in the SSA production mechanism or bubble sizes generated by the breaking wave.
6
7
8
9

10 **5.2 Biological dynamics during the mesocosm experiment**

11

12 One of the most crucial elements of mesocosm experiments to study ocean-atmosphere
13 processes is the stimulation of a phytoplankton bloom, involving all the trophic interactions
14 in the microbial loop between phytoplankton, protozoans, heterotrophic bacteria, and
15 viruses.^{32,66,77,78} Recent efforts have sought to better reproduce the complexity of marine
16 biology while also accurately measuring the turnover of assemblages to better ascribe
17 changes in seawater, SSA composition and properties, and VOC production. An ongoing
18 challenge is the successful stimulation of authentic mesocosms using natural seawater, which
19 varies in biological composition and may not respond immediately to nutrient amendments.
20 During Bloom 3, the addition of the outdoor tank grown in elevated nutrient conditions and
21 natural sunlight provided a richer starter culture for further growth in the wave channel. In the
22 future, enhanced lighting intensity, which more closely mimics natural sunlight, will be
23 implemented to allow bloom formation without this added intervention.
24
25
26
27
28
29
30
31
32

33 The combination of SPCS and microscopy provided a detailed observation of the
34 phytoplankton and microzooplankton dynamic and trophic interactions during the
35 experiment. The phytoplankton assemblages showed a natural succession throughout the
36 course of the experiment, from a diatom-dominated community at the peak of the bloom
37 during the growth phase towards a diatom-aggregate and zooplankton-populated senescent
38 phase. Observation of potential grazing on phytoplankton by microzooplankton and
39 aggregate formation towards the end of the bloom provided insight on the physiological state
40 of the phytoplankton bloom across the experiment (Figure 6). These types of stressors upon
41
42
43
44
45
46
47
48
49
50
51
52
53

1
2
3 phytoplankton may lead to released exudates containing carbon and sulfur that will supply
4 microbial metabolisms, which in turn may influence the production and composition of
5 climate relevant trace gases and the composition of biogenic aerosol.⁷⁹ Future work will
6 compare phytoplankton and VOC concentrations across this study, to screen for specific taxa
7 that may influence VOC production and transformation. The connections between the
8 biological species and the chemical composition of DOM and aerosol will also be the focus
9 of forthcoming SeaSCAPE studies. Further analysis of the functional (e.g. production,
10 enzymes) and community (16S and 18S rDNA amplicon sequencing) adaptation of the
11 marine microbes over the course of the bloom in the bulk seawater, SSML and aerosols will
12 help address some of the chemical changes observed during SeaSCAPE.
13
14
15
16
17
18
19
20
21

22 **5.3 Photochemical VOC production**

23

24 The abiotic production of VOCs from seawater via reactions of surface-present organics
25 with light and oxidants has been recently discussed as a possible source of atmospheric VOCs
26 competitive in emission quantity with marine biology.⁷⁵ Currently, only laboratory
27 measurements of abiotic VOC production have been undertaken, with most utilizing SSML
28 or synthetic organic films doped with terrestrially relevant photosensitizers to enhance yields
29 of irradiation-initiated VOC emission.^{73,80} Here, using unadulterated seawater from our
30 mesocosm experiments, we show small quantities of abiotic, light-driven VOC generation,
31 including cyclic species, but do not maintain sustained emission compared to other laboratory
32 investigations. Lack of sustained emission is likely due to the limited pool of volatile organic
33 species in seawater, which may have been lost through emission and chemical
34 transformation. While the complex mechanisms that control photoinitiated VOC production
35 are poorly understood, mesocosm experiments serve as a valuable bridge between field and
36
37
38
39
40
41
42
43
44
45
46
47
48
49
50
51
52
53

laboratory work towards determining the relative contributions of biotic and abiotic VOC production in the marine environment and will be further pursued.

5.4 Influence of photochemical aging on SSA composition and secondary aerosol formation

Small SSA can be significantly enriched with organic species,⁸¹ which influences their reactivity and water uptake properties.^{24,82} However, the role of atmospheric oxidation processes in transforming the organic chemical composition of SSA remains poorly understood. We found that heterogeneous aging of SSA by OH radical led to significant changes in its morphology, with the total loss of prism-like and aggregate type particles and a large enhancement in core-shell particles. Increased oxidation of organic aerosol has been shown to increase its viscosity, potentially affecting its phase state.^{83,84} This process may have contributed to the change in SSA morphologies observed here. An alternative explanation is that coating of secondary organic species onto the SSA altered its morphology. Future studies are necessary to understand how both of these processes influence SSA phase and morphology, and the potential influence on the climate relevant properties of SSA, such as ice nucleation, water uptake, and light scattering.

6. Conclusions

In summary, wave channels are an important method for understanding the production and properties of marine aerosols and gases under controlled laboratory conditions. Optimization of the wave channel system has enabled even more detailed atmospheric measurements over previous experimental campaigns. In addition, major improvements have been made in the capability to simulate complex seawater biology. The incorporation of oxidation flow reactors has, for the first time, enabled the study of secondary aerosol

1
2
3 formation and photochemical aging of SSA during a large-scale wave channel experiment.
4 Preliminary findings from the SeaSCAPE campaign shed light on the photochemical
5 production of VOCs, impact of atmospheric aging on SSA phase and morphology, and the
6 chemical composition of SMA. Future analysis of the SeaSCAPE dataset is expected to give
7 insight to, among other processes, the nature of marine INPs in both freshly emitted and
8 hetSSA; the potential for both SSA and SMA to serve as CCN in the marine atmosphere; the
9 molecular composition of SSA and its links to biological activity; the identity of unique
10 marine VOCs and possible SOA precursors; and the effect of photochemical aging on the
11 chemical composition of marine aerosols. Oceanic emissions of both gases and particles have
12 profound effects on the climate through their interactions with clouds and solar radiation.
13 Laboratory ocean-atmosphere experiments have and will continue to expand our knowledge
14 of marine aerosols and their influence on a changing climate system.
15
16
17
18
19
20
21
22
23
24
25

26 **Author Contributions:**

27
28 J.S.S., K.J.M, C.L., V.H.G., T.H.B., C.D.C., and K.A.P. conceptualized the experiment.
29 Investigation was conducted by J.S.S., K.J.M, C.L., M.R.A., S.A., C.J.B., E.B.F., D.R.C.,
30 D.D., J.D., L.A.G., C.P.K., D.B.K., L.E.M., B.A.M., D.R.M., C.K.M., A.N.M., C.A.M.,
31 C.M.N., M.A.P., D.P., R.M.C.S., S.S., P.R.T., J.L.W., F.M., and C.D.C. Project
32 administration was performed by C.L. Supervision of the project was conducted by P.J.D.,
33 D.K.F., A.H.G., V.H.G., J.S.J., F.M., T.R.M., J.H.S., A.V.T., T.H.B., C.D.C., and K.A.P. The
34 original draft of the manuscript was written by J.S.S., K.J.M, C.L., M.R.A., S.A., E.B.F.,
35 D.R.C., J.D., L.A.G., C.P.K., D.B.K., L.E.M., B.A.M., C.K.M., M.A.P., P.R.T., J.L.W., F.M.
36 The paper was reviewed and edited by D.P., R.M.C.S., P.J.D., D.K.F., A.H.G., V.H.G.,
37 J.H.S., A.V.T., T.H.B., C.D.C., K.A.P.
38
39
40
41
42
43
44
45
46
47
48
49
50
51
52
53

Conflicts of Interest

There are no conflicts to declare.

Acknowledgements

This material is based upon work supported by the National Science Foundation through the NSF Center for Aerosol Impacts on the Chemistry of the Environment, a Center for Chemical Innovation (CHE-1801971). Thank you to the entire SeaSCAPE team for their hard work throughout the experimental campaign. A full list of participants can be found online: <https://caice.ucsd.edu/experiment-campaigns/>. We thank Tran Nguyen and the Professor Lihini Aluwihare Lab for analysis of the DOC samples. We would like to acknowledge Dr. Pedro Belda-Ferre, Professors Elizabeth Stone, Juan Navea, Mike Tauber, Jim Smith, Pieter Dorrestein, Rob Knight, and Farooq Azam for their contributions to the experiment. Special thanks to Joe Mayer for his assistance with fabricating the ISV and the wave channel paddle system; Professor Mark Young for assisting with the paddle software; Dr. Grant Deane and Dr. Dale Stokes for assistance with wave channel operation; and Rob Klidy and the Hydraulics Laboratory staff. Thank you to Victor Or for designing the TOC graphic.

References

- (1) Boucher, O.; Randall, D.; Artaxo, P.; Bretherton, C.; Feingold, G.; Forster, P.; Kerminen, V. M.; Kondo, Y.; Liao, H.; Lohmann, U.; Rasch, P.; Satheesh, S. K.; Sherwood, S.; Stevens, B.; Zhang, X. Y. Clouds and Aerosols, in *Climate Change 2013: The Physical Science Basis. Contribution of Working Group I to the Fifth Assessment Report of the Intergovernmental Panel on Climate Change*, ed. Stocker, T.F., D. Qin, G.-K. Plattner, M. Tignor, S.K. Allen, J. Boschung, A. Nauels, Y. Xia, V. Bex and P.M. Midgley. Cambridge University Press, Cambridge, United Kingdom and

- 1
2
3 New York, NY, USA, pp. 571-632.
4
- 5 (2) Carslaw, K. S.; Lee, L. a; Reddington, C. L.; Pringle, K. J.; Rap, A; Forster, P. M.;
6 Mann, G. W.; Spracklen, D. V; Woodhouse, M. T.; Regayre, L. A; Pierce, J. R. Large
7 Contribution of Natural Aerosols to Uncertainty in Indirect Forcing. *Nature* **2013**, *503*,
8 67–71.
9
- 10
11 (3) Lewis, E. R.; Schwartz, S. E. *Sea Salt Aerosol Production: Mechanisms, Methods,*
12 *Measurements, and Models--A Critical Review*; American Geophysical Union:
13 Washington D.C., 2004.
14
- 15 (4) Gong, S. L.; Barrie, L. A.; Lazare, M. Canadian Aerosol Module (CAM): A Size-
16 Segregated Simulation of Atmospheric Aerosol Processes for Climate and Air Quality
17 Models 2. Global Sea-Salt Aerosol and Its Budgets. *J. Geophys. Res. Atmos.* **2002**,
18 *107*, 1–14.
19
- 20 (5) Wang, X.; Deane, G. B.; Moore, K. A.; Ryder, O. S.; Stokes, M. D.; Beall, C. M.;
21 Collins, D. B.; Santander, M. V.; Burrows, S. M.; Sultana, C. M.; Prather, K. A. The
22 Role of Jet and Film Drops in Controlling the Mixing State of Submicron Sea Spray
23 Aerosol Particles. *Proc. Natl. Acad. Sci. U. S. A.* **2017**, *114*, 6978–6983.
24
- 25 (6) Quinn, P. K.; Collins, D. B.; Grassian, V. H.; Prather, K. A.; Bates, T. S. Chemistry
26 and Related Properties of Freshly Emitted Sea Spray Aerosol. *Chem. Rev.* **2015**, *115*,
27 4383–4399.
28
- 29 (7) O’Dowd, C. D.; de Leeuw, G. Marine Aerosol Production: A Review of the Current
30 Knowledge. *Philos. Trans. R. Soc. A Math. Phys. Eng. Sci.* **2007**, *365*, 1753–1774.
31
- 32 (8) Prather, K. A.; Bertram, T. H.; Grassian, V. H.; Deane, G. B.; Stokes, M. D.; Demott,
33 P. J.; Aluwihare, L. I.; Palenik, B. P.; Azam, F.; Seinfeld, J. H.; Moffet, R. C.; Molina,
34 M. J.; Cappa, C. D.; Geiger, F. M.; Roberts, G. C.; Russell, L. M.; Ault, A. P.;
35 Baltrusaitis, J.; Collins, D. B.; Corrigan, C. E.; Cuadra-Rodriguez, L. a; Ebben, C. J.;
36 Forestieri, S. D.; Guasco, T. L.; Hersey, S. P.; Kim, M. J.; Lambert, W. F.; Modini, R.
37
38
39
40
41
42
43
44
45
46
47
48
49
50
51
52
53

- 1
2
3 L.; Mui, W.; Pedler, B. E.; Ruppel, M. J.; Ryder, O. S.; Schoepp, N. G.; Sullivan, R.
4 C.; Zhao, D. Bringing the Ocean into the Laboratory to Probe the Chemical
5 Complexity of Sea Spray Aerosol. *Proc. Natl. Acad. Sci. U. S. A.* **2013**, *110*, 7550–
6 7555.
7
8
9
10 (9) Stokes, M. D.; Deane, G. B.; Prather, K.; Bertram, T. H.; Ruppel, M. J.; Ryder, O. S.;
11 Brady, J. M.; Zhao, D. A Marine Aerosol Reference Tank System as a Breaking Wave
12 Analogue for the Production of Foam and Sea-Spray Aerosols. *Atmos. Meas. Tech.*
13 **2013**, *6*, 1085–1094.
14
15
16
17 (10) Stokes, M. D.; Deane, G.; Collins, D. B.; Cappa, C.; Bertram, T.; Dommer, A.; Schill,
18 S.; Forestieri, S.; Survilo, M. A Miniature Marine Aerosol Reference Tank
19 (MiniMART) as a Compact Breaking Wave Analogue. *Atmos. Meas. Tech.* **2016**, *9*,
20 4257–4267.
21
22
23
24 (11) Fuentes, E.; Coe, H.; Green, D.; De Leeuw, G.; McFiggans, G. On the Impacts of
25 Phytoplankton-Derived Organic Matter on the Properties of the Primary Marine
26 Aerosol - Part 1: Source Fluxes. *Atmos. Chem. Phys.* **2010**, *10*, 9295–9317.
27
28
29 (12) Sellegri, K.; O'Dowd, C. D.; Yoon, Y. J.; Jennings, S. G.; de Leeuw, G. Surfactants
30 and Submicron Sea Spray Generation. *J. Geophys. Res. Atmos.* **2006**, *111*, 1–12.
31
32
33 (13) Hultin, K. A. H.; Nilsson, E. D.; Krejci, R.; Mrtensson, E. M.; Ehn, M.; Hagström, Å.;
34 De Leeuw, G. In Situ Laboratory Sea Spray Production during the Marine Aerosol
35 Production 2006 Cruise on the Northeastern Atlantic Ocean. *J. Geophys. Res. Atmos.*
36 **2010**, *115*, 1–19.
37
38
39 (14) Christiansen, S.; Salter, M. E.; Gorokhova, E.; Nguyen, Q. T.; Bilde, M. Sea Spray
40 Aerosol Formation: Laboratory Results on the Role of Air Entrainment, Water
41 Temperature, and Phytoplankton Biomass. *Environ. Sci. Technol.* **2019**.
42
43
44 (15) Salter, M. E.; Nilsson, E. D.; Butcher, A.; Bilde, M. On the Seawater Temperature
45 Dependence of the Sea Spray Aerosol Generated by a Continuous Plunging Jet. *J.*
46
47
48
49
50
51
52
53

- 1
2
3
4
5
6
7
8
9
10
11
12
13
14
15
16
17
18
19
20
21
22
23
24
25
26
27
28
29
30
31
32
33
34
35
36
37
38
39
40
41
42
43
44
45
46
47
48
49
50
51
52
53
- Geophys. Res.* **2014**, *119*, 9052–9072.
- (16) Collins, D. B.; Zhao, D. F.; Ruppel, M. J.; Laskina, O.; Grandquist, J. R.; Modini, R. L.; Stokes, M. D.; Russell, L. M.; Bertram, T. H.; Grassian, V. H.; Deane, G. B.; Prather, K. A. Direct Aerosol Chemical Composition Measurements to Evaluate the Physicochemical Differences between Controlled Sea Spray Aerosol Generation Schemes. *Atmos. Meas. Tech.* **2014**, *7*, 3667–3683.
- (17) Mayer, K. J.; Sauer, J. S.; Dinasquet, J.; Prather, K. A. CAICE Studies: Insights from a Decade of Ocean – Atmosphere Experiments in the Laboratory. *Acc. Chem. Res.* **2020**, *53*, 2510-2520.
- (18) DeMott, P. J.; Hill, T. C. J.; McCluskey, C. S.; Prather, K. A.; Collins, D. B.; Sullivan, R. C.; Ruppel, M. J.; Mason, R. H.; Irish, V. E.; Lee, T.; Hwang, C. Y.; Rhee, T. S.; Snider, J. R.; McMeeking, G. R.; Dhaniyala, S.; Lewis, E. R.; Wentzell, J. J. B.; Abbatt, J.; Lee, C.; Sultana, C. M.; Ault, A. P.; Axson, J. L.; Diaz Martinez, M.; Venero, I.; Santos-Figueroa, G.; Stokes, M. D.; Deane, G. B.; Mayol-Bracero, O. L.; Grassian, V. H.; Bertram, T. H.; Bertram, A. K.; Moffett, B. F.; Franc, G. D. Sea Spray Aerosol as a Unique Source of Ice Nucleating Particles. *Proc. Natl. Acad. Sci.* **2015**, *113*, 201514034.
- (19) Michaud, J. M.; Thompson, L. R.; Kaul, D.; Espinoza, J. L.; Richter, R. A.; Xu, Z. Z.; Lee, C.; Pham, K. M.; Beall, C. M.; Malfatti, F.; Azam, F.; Knight, R.; Burkart, M. D.; Dupont, C. L.; Prather, K. A. Taxon-Specific Aerosolization of Bacteria and Viruses in an Experimental Ocean-Atmosphere Mesocosm. *Nat. Commun.* **2018**, *9*.
- (20) Wang, X.; Sultana, C. M.; Trueblood, J.; Hill, T. C. J.; Malfatti, F.; Lee, C.; Laskina, O.; Moore, K. A.; Beall, C. M.; McCluskey, C. S.; Cornwell, G. C.; Zhou, Y.; Cox, J. L.; Pendergraft, M. A.; Santander, M. V.; Bertram, T. H.; Cappa, C. D.; Azam, F.; DeMott, P. J.; Grassian, V. H.; Prather, K. A. Microbial Control of Sea Spray Aerosol Composition: A Tale of Two Blooms. *ACS Cent. Sci.* **2015**, *1*, 124–131.

- 1
2
3
4
5
6
7
8
9
10
11
12
13
14
15
16
17
18
19
20
21
22
23
24
25
26
27
28
29
30
31
32
33
34
35
36
37
38
39
40
41
42
43
44
45
46
47
48
49
50
51
52
53
- (21) Kim, M. J.; Michaud, J. M.; Williams, R.; Sherwood, B. P.; Pomeroy, R.; Azam, F.; Burkart, M.; Bertram, T. H. Bacterial-Driven Production of Nitrates in Seawater. *Geophys. Res. Lett.* **2015**, *42*, 1–8.
- (22) Patterson, J. P.; Collins, D. B.; Michaud, J. M.; Axson, J. L.; Sultana, C. M.; Moser, T.; Dommer, A. C.; Conner, J.; Grassian, V. H.; Stokes, M. D.; Deane, G. B.; Evans, J. E.; Burkart, M. D.; Prather, K. A.; Gianneschi, N. C. Sea Spray Aerosol Structure and Composition Using Cryogenic Transmission Electron Microscopy. *ACS Cent. Sci.* **2016**, *2*, 40–47.
- (23) Lee, H. D.; Wigley, S.; Lee, C.; Or, V. W.; Hasenecz, E. S.; Stone, E. A.; Grassian, V. H.; Prather, K. A.; Tivanski, A. V. Physicochemical Mixing State of Sea Spray Aerosols: Morphologies Exhibit Size Dependence. *ACS Earth Sp. Chem.* **2020**, *4*, 1604–1611.
- (24) Ryder, O. S.; Campbell, N. R.; Morris, H.; Forestieri, S.; Ruppel, M. J.; Cappa, C.; Tivanski, A.; Prather, K.; Bertram, T. H. Role of Organic Coatings in Regulating N₂O₅ Reactive Uptake to Sea Spray Aerosol. *J. Phys. Chem. A* **2015**, *119*, 11683–11692.
- (25) Ault, A. P.; Guasco, T. L.; Ryder, O. S.; Baltrusaitis, J.; Cuadra-Rodriguez, L. A.; Collins, D. B.; Ruppel, M. J.; Bertram, T. H.; Prather, K. A.; Grassian, V. H. Inside versus Outside: Ion Redistribution in Nitric Acid Reacted Sea Spray Aerosol Particles as Determined by Single Particle Analysis. *J. Am. Chem. Soc.* **2013**, *135*, 14528–14531.
- (26) Trueblood, J. V.; Estillore, A. D.; Lee, C.; Dowling, J. A.; Prather, K. A.; Grassian, V. H. Heterogeneous Chemistry of Lipopolysaccharides with Gas-Phase Nitric Acid: Reactive Sites and Reaction Pathways. *J. Phys. Chem. A* **2016**, *120*, 6444–6450.
- (27) Estillore, A. D.; Trueblood, J. V.; Grassian, V. H. Atmospheric Chemistry of Bioaerosols: Heterogeneous and Multiphase Reactions with Atmospheric Oxidants and

- 1
2
3 Other Trace Gases. *Chem. Sci.* **2016**, *7*, 6604–6616.
4
5 (28) Trueblood, J. V.; Wang, X.; W. Or, V.; R. Alves, M.; V. Santander, M.; A. Prather, K.;
6 H. Grassian, V. The Old and the New: Aging of Sea Spray Aerosol and Formation of
7 Secondary Marine Aerosol through OH Oxidation Reactions. *ACS Earth Sp. Chem.*
8 **2019**, *3*, 2307–2314.
9
10 (29) Mayer, K. J.; Wang, X.; Santander, M. V.; Mitts, B. A.; Sauer, J. S.; Sultana, C. M.;
11 Cappa, C. D.; Prather, K. A. Secondary Marine Aerosol Plays a Dominant Role over
12 Primary Sea Spray Aerosol in Cloud Formation. *ACS Cent. Sci.* **2020**, *6*, 2259–2266.
13
14 (30) Schneider, S. R.; Collins, D. B.; Lim, C. Y.; Zhu, L.; Abbatt, J. P. D. Formation of
15 Secondary Organic Aerosol from the Heterogeneous Oxidation by Ozone of a
16 Phytoplankton Culture. *ACS Earth Sp. Chem.* **2019**, *3*, 2298–2306.
17
18 (31) Bouvet, M.; Hoepffner, N.; Dowell, M. D. Parameterization of a Spectral Solar
19 Irradiance Model for the Global Ocean Using Multiple Satellite Sensors. *J. Geophys.*
20 *Res. Ocean.* **2002**, *107*, 8–18.
21
22 (32) Lee, C.; Sultana, C. M.; Collins, D. B.; Santander, M. V.; Axson, J. L.; Malfatti, F.;
23 Cornwell, G. C.; Grandquist, J. R.; Deane, G. B.; Stokes, M. D.; Azam, F.; Grassian,
24 V. H.; Prather, K. a. Advancing Model Systems for Fundamental Laboratory Studies
25 of Sea Spray Aerosol Using the Microbial Loop. *J. Phys. Chem. A* **2015**,
26 150805131932006.
27
28 (33) Guillard, R. R. L.; Ryther, J. H. Studies of Marine Planktonic Diatoms. *Can. J.*
29 *Microbiol.* **1962**, *8*, 229–238.
30
31 (34) Kang, E.; Root, M. J.; Brune, W. H. Introducing the Concept of Potential Aerosol
32 Mass (PAM). *Atmos. Chem. Phys.* **2007**, *7*, 5727-5744.
33
34 (35) Lambe, A. T.; Ahern, A. T.; Williams, L. R.; Slowik, J. G.; Wong, J. P. S.; Abbatt, J.
35 P. D.; Brune, W. H.; Ng, N. L.; Wright, J. P.; Croasdale, D. R.; Worsnop, D. R.;
36 Davidovits, P.; Onasch, T. B. Characterization of Aerosol Photooxidation Flow
37
38
39
40
41
42
43
44
45
46
47
48
49
50
51
52
53

- Reactors: Heterogeneous Oxidation, Secondary Organic Aerosol Formation and Cloud Condensation Nuclei Activity Measurements. *Atmos. Meas. Tech.* **2011**, *4*, 445–461.
- (36) Chen, W.-C.; Marcus, R. A. On the Theory of the Reaction Rate of Vibrationally Excited CO Molecules with OH Radicals. *J. Chem. Phys.* **2006**, *124*, 024306.
- (37) Wolfe, G. M.; Nicely, J. M.; St. Clair, J. M.; Hanisco, T. F.; Liao, J.; Oman, L. D.; Brune, W. B.; Miller, D.; Thames, A.; González Abad, G.; Ryerson, T. B.; Thompson, C. R.; Peischl, J.; McKain, K.; Sweeney, C.; Wennberg, P. O.; Kim, M.; Crouse, J. D.; Hall, S. R.; Ullmann, K.; Diskin, G.; Bui, P.; Chang, C.; Dean-Day, J. Mapping Hydroxyl Variability throughout the Global Remote Troposphere via Synthesis of Airborne and Satellite Formaldehyde Observations. *Proc. Natl. Acad. Sci.* **2019**, *116*, 11171–11180.
- (38) Lee, H. D.; Kaluarachchi, C. P.; Hasenecz, E. S.; Zhu, J. Z.; Popa, E.; Stone, E. A.; Tivanski, A. V. Effect of Dry or Wet Substrate Deposition on the Organic Volume Fraction of Core-Shell Aerosol Particles. *Atmos. Meas. Tech.* **2019**, *12*, 2033–2042.
- (39) Lee, H. D.; Morris, H. S.; Laskina, O.; Sultana, C. M.; Lee, C.; Jayarathne, T.; Cox, J. L.; Wang, X.; Hasenecz, E. S.; Demott, P. J.; Bertram, T. H.; Cappa, C. D.; Stone, E. A.; Prather, K. A.; Grassian, V. H.; Tivanski, A. V. Organic Enrichment, Physical Phase State, and Surface Tension Depression of Nascent Core-Shell Sea Spray Aerosols during Two Phytoplankton Blooms. *ACS Earth Sp. Chem.* **2020**, *4*, 650–660.
- (40) DeCarlo, P. F.; Kimmel, J. R.; Trimborn, A.; Northway, M. J.; Jayne, J. T.; Aiken, A. C.; Gonin, M.; Fuhrer, K.; Horvath, T.; Docherty, K. S.; Worsnop, D. R.; Jimenez, J. L. Field-Deployable, High-Resolution, Time-of-Flight Aerosol Mass Spectrometer. *Anal. Chem.* **2006**, *78*, 8281–8289.
- (41) Kercher, J. P.; Riedel, T. P.; Thornton, J. A. Chlorine Activation by N₂O₅: Simultaneous, in Situ Detection of ClNO₂ and N₂O₅ by Chemical Ionization Mass Spectrometry. *Atmos. Meas. Tech.* **2009**, *2*, 193–204.

- 1
2
3 (42) Kim, M. J.; Zoerb, M. C.; Campbell, N. R.; Zimmermann, K. J.; Blomquist, B. W.;
4 Huebert, B. J.; Bertram, T. H. Revisiting Benzene Cluster Cations for the Chemical
5 Ionization of Dimethyl Sulfide and Select Volatile Organic Compounds. *Atmos. Meas.*
6 *Tech.* **2016**, *9*, 1473–1484.
7
8
9
10 (43) Lavi, A.; Vermeuel, M. P.; Novak, G. A.; Bertram, T. H. The Sensitivity of Benzene
11 Cluster Cation Chemical Ionization Mass Spectrometry to Select Biogenic Terpenes.
12 *Atmos. Meas. Tech.* **2018**, *11*, 3251–3262.
13
14
15 (44) Krechmer, J.; Lopez-Hilfiker, F.; Koss, A.; Hutterli, M.; Stoermer, C.; Deming, B.;
16 Kimmel, J.; Warneke, C.; Holzinger, R.; Jayne, J.; Worsnop, D.; Fuhrer, K.; Gonin,
17 M.; De Gouw, J. Evaluation of a New Reagent-Ion Source and Focusing Ion-Molecule
18 Reactor for Use in Proton-Transfer-Reaction Mass Spectrometry. *Anal. Chem.* **2018**,
19 *90*, 12011–12018.
20
21
22
23
24 (45) Roveretto, M.; Li, M.; Hayeck, N.; Brüggemann, M.; Emmelin, C.; Perrier, S.; George,
25 C. Real-Time Detection of Gas-Phase Organohalogenes from Aqueous Photochemistry
26 Using Orbitrap Mass Spectrometry. *ACS Earth Sp. Chem.* **2019**, *3*, 329–334.
27
28
29 (46) Hatch, L. E.; Jen, C. N.; Kreisberg, N. M.; Selimovic, V.; Yokelson, R. J.; Stamatis,
30 C.; York, R. A.; Foster, D.; Stephens, S. L.; Goldstein, A. H.; Barsanti, K. C. Highly
31 Speciated Measurements of Terpenoids Emitted from Laboratory and Mixed-Conifer
32 Forest Prescribed Fires. *Environ. Sci. Technol.* **2019**, *53*, 9418–9428.
33
34
35
36 (47) Carlson, D. J. Surface Microlayer Phenolic Enrichments Indicate Sea Surface Slicks.
37 *Nature* **1982**, *296*, 426–429.
38
39
40 (48) Cunliffe, M.; Wurl, O. Sampling the Sea Surface Microlayer. In *Hydrocarbon and*
41 *Lipid Microbiology Protocols. Springer Protocols Handbooks*; McGenity, T., Timmis,
42 K., Nogales, B., Eds.; Springer, Berlin, Heidelberg, 2015.
43
44
45 (49) Worton, D. R.; Decker, M.; Isaacman-VanWertz, G.; Chan, A. W. H.; Wilson, K. R.;
46 Goldstein, A. H. Improved Molecular Level Identification of Organic Compounds
47
48
49
50
51
52
53

- 1
2
3 Using Comprehensive Two-Dimensional Chromatography, Dual Ionization Energies
4 and High Resolution Mass Spectrometry. *Analyst* **2017**, *142*, 2395–2403.
- 5
6
7 (50) Holm-Hansen, O.; Lorenzen, C. J.; Holmes, R. W.; Strickland, J. D. H. Fluorometric
8 Determination of Chlorophyll. *ICES J. Mar. Sci.* **1965**, *30*, 3–15.
- 9
10 (51) Menzel, D. W.; Vaccaro, R. F. The Measurement of Dissolved Organic Carbon in
11 Seawater. *Limnol. Oceanogr.* **1964**, *9*, 138–142.
- 12
13 (52) Utermöhl, von H. Neue Wege in Der Quantitativen Erfassung Des Plankton. (Mit
14 Besonderer Berücksichtigung Des Ultraplanktons). *Int. Verein. Theor. Angew. Limnol.*,
15 **1931**, *5*, 567–596.
- 16
17 (53) Orenstein, E. C.; Ratelle, D.; Briseño-Avena, C.; Carter, M.; Franks, P. J. S.; Jaffe, J.
18 S.; Roberts, P. L. D. The Scripps Plankton Camera System: A Framework and
19 Platform for in Situ Microscopy. *Limnol. Oceanogr. Methods* **2020**, *18*, 681–695.
- 20
21 (54) Gasol, J. M.; Del Giorgio, P. A. Using Flow Cytometry for Counting Natural
22 Planktonic Bacteria and Understanding the Structure of Planktonic Bacterial
23 Communities. *Sci. Mar.* **2000**, *64*, 197–224.
- 24
25 (55) Brussaard, C. P. D. Optimization of Procedures for Counting Viruses by Flow
26 Cytometry. *Appl. Environ. Microbiol.* **2004**, *70*, 1506–1513.
- 27
28 (56) Marie, D.; Partensky, F.; Jacquet, S.; Vaulot, D. Enumeration and Cell Cycle Analysis
29 of Natural Populations of Marine Picoplankton by Flow Cytometry Using the Nucleic
30 Acid Stain SYBR Green I. *Appl. Environ. Microbiol.* **1997**, *63*, 186–193.
- 31
32 (57) Noble, R. T.; Fuhrman, J. A. Use of SYBR Green I for Rapid Epifluorescence Counts
33 of Marine Viruses and Bacteria. *Aquat. Microb. Ecol.* **1998**, *14*, 113–118.
- 34
35 (58) Olson, R. J.; Chisholm, S. W.; Zettler, E. R.; Armbrust, E. V. Pigments, Size, and
36 Distributions of Synechococcus in the North Atlantic and Pacific Oceans. *Limnol.*
37 *Oceanogr.* **1990**, *35*, 45–58.
- 38
39 (59) Hering, S. V.; Spielman, S. R.; Lewis, G. S. Moderated, Water-Based, Condensational
40
41
42
43
44
45
46
47
48
49
50
51
52
53

- 1
2
3 Particle Growth in a Laminar Flow. *Aerosol Sci. Technol.* **2014**, *48*, 401–408.
- 4
5 (60) Marie, D.; Rigaut-Jalabert, F.; Vaulot, D. An Improved Protocol for Flow Cytometry
6 Analysis of Phytoplankton Cultures and Natural Samples. *Cytom. Part A* **2014**, *85*,
7 962–968.
- 8
9
10 (61) Christaki, U.; Courties, C.; Massana, R.; Catala, P.; Lebaron, P.; Gasol, J. M.; Zubkov,
11 M. V. Optimized Routine Flow Cytometric Enumeration of Heterotrophic Flagellates
12 Using SYBR Green I. *Limnol. Oceanogr. Methods* **2011**, *9*, 329–339.
- 13
14
15 (62) Ye, C.; Zhou, X.; Pu, D.; Stutz, J.; Festa, J.; Spolaor, M.; Tsai, C.; Cantrell, C.;
16 Mauldin, R. L.; Campos, T.; Weinheimer, A.; Hornbrook, R. S.; Apel, E. C.; Guenther,
17 A.; Kaser, L.; Yuan, B.; Karl, T.; Haggerty, J.; Hall, S.; Ullmann, K.; Smith, J. N.;
18 Ortega, J.; Knote, C. Rapid Cycling of Reactive Nitrogen in the Marine Boundary
19 Layer. *Nature* **2016**, *532*, 489–491.
- 20
21
22
23
24 (63) Seinfeld, J. H.; Pandis, S. N. *Atmospheric Chemistry and Physics: From Air Pollution*
25 *to Climate Change*, Third Ed.; John Wiley & Sons, Inc.: Hoboken, New Jersey, 2016.
- 26
27 (64) Boylan, P.; Helmig, D.; Oltmans, S. Ozone in the Atlantic Ocean Marine Boundary
28 Layer. *Elem. Sci. Anthr.* **2015**, *3*, 1–13.
- 29
30
31 (65) Wakeham, S. G.; Canuel, E. A.; Doering, P. H. Geochemistry of Volatile Organic
32 Compounds in Seawater: Mesocosm Experiments with ¹⁴C-Model Compounds.
33 *Geochim. Cosmochim. Acta* **1986**, *50*, 1163–1172.
- 34
35
36 (66) Buchan, A.; LeClerc, G. R.; Gulvik, C. A.; González, J. M. Master Recyclers: Features
37 and Functions of Bacteria Associated with Phytoplankton Blooms. *Nat. Rev.*
38 *Microbiol.* **2014**, *12*, 686–698.
- 39
40
41 (67) Hermabessiere, L.; Dehaut, A.; Paul-Pont, I.; Lacroix, C.; Jezequel, R.; Soudant, P.;
42 Duflos, G. Occurrence and Effects of Plastic Additives on Marine Environments and
43 Organisms: A Review. *Chemosphere* **2017**, *182*, 781–793.
- 44
45
46 (68) Gaw, S.; Thomas, K. V.; Hutchinson, T. H. Sources, Impacts and Trends of
47
48
49
50
51
52
53

- 1
2
3
4
5
6
7
8
9
10
11
12
13
14
15
16
17
18
19
20
21
22
23
24
25
26
27
28
29
30
31
32
33
34
35
36
37
38
39
40
41
42
43
44
45
46
47
48
49
50
51
52
53
- Pharmaceuticals in the Marine and Coastal Environment. *Philos. Trans. R. Soc. B Biol. Sci.* **2014**, *369*.
- (69) Forestieri, S. D.; Moore, K. A.; Martinez Borrero, R.; Wang, A.; Stokes, M. D.; Cappa, C. D. Temperature and Composition Dependence of Sea Spray Aerosol Production. *Geophys. Res. Lett.* **2018**, *45*, 7218–7225.
- (70) Leu, M. T.; Timonen, R. S.; Keyser, L. F.; Yung, Y. L. Heterogeneous Reactions of $\text{HNO}_3(\text{g}) + \text{NaCl}(\text{s}) \rightarrow \text{HCl}(\text{g}) + \text{NaNO}_3(\text{s})$ and $\text{N}_2\text{O}_5(\text{g}) + \text{NaCl}(\text{s}) \rightarrow \text{ClNO}_2(\text{g}) + \text{NaNO}_3(\text{s})$. *J. Phys. Chem.* **1995**, *99*, 13203–13212.
- (71) Gard, E. E.; Kleeman, M. J.; Gross, D. S.; Hughes, L. S.; Allen, J. O.; Morrical, B. D.; Ferguson, D. P.; Dienes, T.; Gälli, M. E.; Johnson, R. J.; Cass, G. R.; Prather, K. A. Direct Observation of Heterogeneous Chemistry in the Atmosphere. *Science* **1998**, *279*, 1184–1187.
- (72) Ault, A. P.; Guasco, T. L.; Baltrusaitis, J.; Ryder, O. S.; Trueblood, J. V.; Collins, D. B.; Ruppel, M. J.; Cuadra-Rodriguez, L. A.; Prather, K. A.; Grassian, V. H. Heterogeneous Reactivity of Nitric Acid with Nascent Sea Spray Aerosol: Large Differences Observed between and within Individual Particles. *J. Phys. Chem. Lett.* **2014**, *5*, 2493–2500.
- (73) Ciuraru, R.; Fine, L.; Pinxteren, M. Van; D'Anna, B.; Herrmann, H.; George, C. Unravelling New Processes at Interfaces: Photochemical Isoprene Production at the Sea Surface. *Environ. Sci. Technol.* **2015**, *49*, 13199–13205.
- (74) Kameyama, S.; Tanimoto, H.; Inomata, S.; Suzuki, K.; Komatsu, D. D.; Hirota, A.; Konno, U. T. A.; Tsunogai, U. Application of PTR-MS to an Incubation Experiment of the Marine Diatom *Thalassiosira Pseudonana*. *Geochem. J.* **2011**, *45*, 355–363.
- (75) Novak, G. A.; Bertram, T. H. Reactive VOC Production from Photochemical and Heterogeneous Reactions Occurring at the Air-Ocean Interface. *Acc. Chem. Res.* **2020**, *53*, 1014–1023.

- 1
2
3 (76) Ray, K. K.; Lee, H. D.; Gutierrez, M. A.; Chang, F. J.; Tivanski, A. V. Correlating 3D
4 Morphology, Phase State, and Viscoelastic Properties of Individual Substrate-
5 Deposited Particles. *Anal. Chem.* **2019**, *91*, 7621–7630.
6
7
8 (77) Pomeroy, L. R.; le Williams, P. J. B.; Azam, F.; Hobbie, J. E. The Microbial Loop.
9 *Oceanography* **2007**, *20*, 28–33.
10
11 (78) Azam, F.; Fenchel, T.; Field, J.; Gray, J.; Meyer-Reil, L.; Thingstad, F. The Ecological
12 Role of Water-Column Microbes in the Sea. *Mar. Ecol. Prog. Ser.* **1983**, *10*, 257–263.
13
14 (79) Ksionzek, K. B.; Lechtenfeld, O. J.; McCallister, S. L.; Schmitt-Kopplin, P.; Geuer, J.
15 K.; Geibert, W.; Koch, B. P. Dissolved Organic Sulfur in the Ocean: Biogeochemistry
16 of a Petagram Inventory. *Science* **2016**, *354*, 456–459.
17
18 (80) Trueblood, J. V.; Alves, M. R.; Power, D.; Santander, M. V.; Cochran, R. E.; Prather,
19 K. A.; Grassian, V. H. Shedding Light on Photosensitized Reactions within Marine-
20 Relevant Organic Thin Films. *ACS Earth Sp. Chem.* **2019**, *3*, 1614–1623.
21
22 (81) O’Dowd, C. D.; Facchini, M. C.; Cavalli, F.; Ceburnis, D.; Mircea, M.; Decesari, S.;
23 Fuzzi, S.; Young, J. Y.; Putaud, J. P. Biogenically Driven Organic Contribution to
24 Marine Aerosol. *Nature* **2004**, *431*, 676–680.
25
26 (82) Estillore, A. D.; Morris, H. S.; Or, V. W.; Lee, H. D.; Alves, M. R.; Marciano, M. A.;
27 Laskina, O.; Qin, Z.; Tivanski, A. V.; Grassian, V. H. Linking Hygroscopicity and the
28 Surface Microstructure of Model Inorganic Salts, Simple and Complex Carbohydrates,
29 and Authentic Sea Spray Aerosol Particles. *Phys. Chem. Chem. Phys.* **2017**, *19*,
30 21101–21111.
31
32 (83) Saukko, E.; Lambe, A. T.; Massoli, P.; Koop, T.; Wright, J. P.; Croasdale, D. R.;
33 Pedernera, D. A.; Onasch, T. B.; Laaksonen, A.; Davidovits, P.; Worsnop, D. R.;
34 Virtanen, A. Humidity-Dependent Phase State of SOA Particles from Biogenic and
35 Anthropogenic Precursors. *Atmos. Chem. Phys.* **2012**, *12*, 7517–7529.
36
37 (84) Athanasiadis, A.; Fitzgerald, C.; Davidson, N. M.; Giorio, C.; Botchway, S. W.; Ward,
38
39
40
41
42
43
44
45
46
47
48
49
50
51
52
53

- 1
2
3 A. D.; Kalberer, M.; Pope, F. D.; Kuimova, M. K. Dynamic Viscosity Mapping of the
4 Oxidation of Squalene Aerosol Particles. *Phys. Chem. Chem. Phys.* **2016**, *18*, 30385–
5 30393.
6
7
8 (85) Shen, S.; Jaques, P. A.; Zhu, Y.; Geller, M. D.; Sioutas, C. Evaluation of the SMPS-
9 APS System as a Continuous Monitor for Measuring PM_{2.5}, PM₁₀ and Coarse
10 (PM_{2.5-10}) Concentrations. *Atmos. Environ.* **2002**, *36*, 3939–3950.
11
12 (86) Peters, T. M.; Leith, D. Concentration Measurement and Counting Efficiency of the
13 Aerodynamic Particle Sizer 3321. *J. Aerosol Sci.* **2003**, *34*, 627–634.
14
15 (87) Lopez-Yglesias, X. F.; Yeung, M. C.; Dey, S. E.; Brechtel, F. J.; Chan, C. K.
16 Performance Evaluation of the Brechtel Mfg. Humidified Tandem Differential
17 Mobility Analyzer (BMI HTDMA) for Studying Hygroscopic Properties of Aerosol
18 Particles. *Aerosol Sci. Technol.* **2014**, *48*, 969–980.
19
20 (88) Hering, S. V.; Lewis, G. S.; Spielman, S. R.; Eiguren-Fernandez, A. A MAGIC
21 Concept for Self-Sustained, Water-Based, Ultrafine Particle Counting. *Aerosol Sci.*
22 *Technol.* **2019**, *53*, 63–72.
23
24 (89) Gard, E.; Mayer, J. E.; Morrical, B. D.; Dienes, T.; Fergenson, D. P.; Prather, K. a.
25 Real-Time Analysis of Individual Atmospheric Aerosol Particles: Design and
26 Performance of a Portable ATOFMS. *Anal. Chem.* **1997**, *69*, 4083–4091.
27
28 (90) Voisin, D.; Smith, J. N.; Sakurai, H.; McMurry, P. H.; Eisele, F. L. Thermal
29 Desorption Chemical Ionization Mass Spectrometer for Ultrafine Particle Chemical
30 Composition. *Aerosol Sci. Technol.* **2003**, *37*, 471–475.
31
32 (91) Smith, J. N.; Moore, K. F.; McMurry, P. H.; Eisele, F. L. Atmospheric Measurements
33 of Sub-20 Nm Diameter Particle Chemical Composition by Thermal Desorption
34 Chemical Ionization Mass Spectrometry. *Aerosol Sci. Technol.* **2004**, *38*, 100–110.
35
36 (92) Lopez-Hilfiker, F. D.; Pospisilova, V.; Huang, W.; Kalberer, M.; Mohr, C.; Stefenelli,
37 G.; Thornton, J. A.; Baltensperger, U.; Prevot, A. S. H.; Slowik, J. G. An Extractive
38
39
40
41
42
43
44
45
46
47
48
49
50
51
52
53

- 1
2
3 Electro spray Ionization Time-of-Flight Mass Spectrometer (EESI-TOF) for Online
4 Measurement of Atmospheric Aerosol Particles. *Atmos. Meas. Tech.* **2019**, *12*, 4867–
5 4886.
6
7
8
9 (93) Roberts, G. C.; Nenes, A. A Continuous-Flow Streamwise Thermal-Gradient CCN
10 Chamber for Atmospheric Measurements. *Aerosol Sci. Technol.* **2005**, *39*, 206–221.
11
12 (94) Jain, S.; Petrucci, G. A. A New Method to Measure Aerosol Particle Bounce Using a
13 Cascade Electrical Low Pressure Impactor. *Aerosol Sci. Technol.* **2015**, *49*, 390–399.
14
15 (95) Demott, P. J.; Prenni, A. J.; McMeeking, G. R.; Sullivan, R. C.; Petters, M. D.; Tobo,
16 Y.; Niemand, M.; Möhler, O.; Snider, J. R.; Wang, Z.; Kreidenweis, S. M. Integrating
17 Laboratory and Field Data to Quantify the Immersion Freezing Ice Nucleation Activity
18 of Mineral Dust Particles. *Atmos. Chem. Phys.* **2015**, *15*, 393–409.
19
20
21
22 (96) Gabey, A. M.; Stanley, W. R.; Gallagher, M. W.; Kaye, P. H. The Fluorescence
23 Properties of Aerosol Larger than 0.8 μ in Urban and Tropical Rainforest Locations.
24 *Atmos. Chem. Phys.* **2011**, *11*, 5491–5504.
25
26
27
28 (97) Perkins, R. J.; Gillette, S. M.; Hill, T. C. J.; Demott, P. J. The Labile Nature of Ice
29 Nucleation by Arizona Test Dust. *ACS Earth Sp. Chem.* **2020**, *4*, 133–141.
30
31
32 (98) Cochran, R. E.; Laskina, O.; Jayarathne, T.; Laskin, A.; Laskin, J.; Lin, P.; Sultana, C.;
33 Lee, C.; Moore, K. A.; Cappa, C. D.; Bertram, T. H.; Prather, K. A.; Grassian, V. H.;
34 Stone, E. A. Analysis of Organic Anionic Surfactants in Fine and Coarse Fractions of
35 Freshly Emitted Sea Spray Aerosol. *Environ. Sci. Technol.* **2016**, *50*, 2477–2486.
36
37
38 (99) Hettiyadura, A. P. S.; Jayarathne, T.; Baumann, K.; Goldstein, A. H.; De Gouw, J. A.;
39 Koss, A.; Keutsch, F. N.; Skog, K.; Stone, E. A. Qualitative and Quantitative Analysis
40 of Atmospheric Organosulfates in Centreville, Alabama. *Atmos. Chem. Phys.* **2017**, *17*,
41 1343–1359.
42
43
44
45 (100) Lee, H. D.; Ray, K. K.; Tivanski, A. V. Solid, Semisolid, and Liquid Phase States of
46 Individual Submicrometer Particles Directly Probed Using Atomic Force Microscopy.
47
48
49
50
51
52
53

- 1
2
3
4
5
6
7
8
9
10
11
12
13
14
15
16
17
18
19
20
21
22
23
24
25
26
27
28
29
30
31
32
33
34
35
36
37
38
39
40
41
42
43
44
45
46
47
48
49
50
51
52
53
- Anal. Chem.* **2017**, *89*, 12720–12726.
- (101) Or, V. W.; Estillore, A. D.; Tivanski, A. V.; Grassian, V. H. Lab on a Tip: Atomic Force Microscopy-Photothermal Infrared Spectroscopy of Atmospherically Relevant Organic/Inorganic Aerosol Particles in the Nanometer to Micrometer Size Range. *Analyst* **2018**, *143*, 2765–2774.
- (102) Mael, L. E.; Busse, H.; Grassian, V. H. Measurements of Immersion Freezing and Heterogeneous Chemistry of Atmospherically Relevant Single Particles with Micro-Raman Spectroscopy. *Anal. Chem.* **2019**, *91*, 11138–11145.
- (103) Angle, K. J.; Crocker, D. R.; Simpson, R. M. C.; Mayer, K. J.; Garofalo, L. A.; Moore, A. N.; Mora Garcia, S. L.; Or, V. W.; Srinivasan, S.; Farhan, M.; Sauer, J. S.; Lee, C.; Pothier, M. A.; Farmer, D. K.; Martz, T. R.; Bertram, T. H.; Cappa, C. D.; Prather, K. A.; Grassian, V. H. Acidity across the Interface from the Ocean Surface to Sea Spray Aerosol. *Proc. Natl. Acad. Sci. U. S. A.* **2021**, *118*, 1–6.
- (104) Petras, D.; Koester, I.; Da Silva, R.; Stephens, B. M.; Haas, A. F.; Nelson, C. E.; Kelly, L. W.; Aluwihare, L. I.; Dorrestein, P. C. High-Resolution Liquid Chromatography Tandem Mass Spectrometry Enables Large Scale Molecular Characterization of Dissolved Organic Matter. *Front. Mar. Sci.* **2017**, *4*, 405.
- (105) Hoppe, H. G. Significance of Exoenzymatic Activities in the Ecology of Brackish Water: Measurements by Means of Methylumbelliferyl-Substrates. *Mar. Ecol. Prog. Ser.* **1983**, *11*, 299–308.
- (106) Crocker, D. R.; Hernandez, R. E.; Huang, H. D.; Pendergraft, M. A.; Cao, R.; Dai, J.; Morris, C. K.; Deane, G. B.; Prather, K. A.; Thiemens, M. H. Biological Influence on ¹³C and Organic Composition of Nascent Sea Spray Aerosol. *ACS Earth Sp. Chem.* **2020**, *4*, 1686–1699.
- (107) Wei, Y.; Jiao, Y.; An, D.; Li, D.; Li, W.; Wei, Q. Review of Dissolved Oxygen Detection Technology: From Laboratory Analysis to Online Intelligent Detection.

- 1
2
3 *Sensors* **2019**, *19*.
- 4
5 (108) Walters, W.; Hyde, E. R.; Berg-Lyons, D.; Ackermann, G.; Humphrey, G.; Parada, A.;
6 Gilbert, J. A.; Jansson, J. K.; Caporaso, J. G.; Fuhrman, J. A.; Apprill, A.; Knight, R.
7 Improved Bacterial 16S rRNA Gene (V4 and V4-5) and Fungal Internal Transcribed
8 Spacer Marker Gene Primers for Microbial Community Surveys. *mSystems* **2016**, *1*,
9 e00009-15.
- 10
11
12
13 (109) Christaki, U.; Courties, C.; Massana, R.; Catala, P.; Lebaron, P.; Gasol, J. M.; Zubkov,
14 M. V. Optimized Routine Flow Cytometric Enumeration of Heterotrophic Flagellates
15 Using SYBR Green I. *Limnol. Oceanogr. Methods* **2011**, *9*, 329–339.
- 16
17
18 (110) Minich, J. J.; Zhu, Q.; Janssen, S.; Hendrickson, R.; Amir, A.; Vetter, R.; Hyde, J.;
19 Doty, M. M.; Stillwell, K.; Benardini, J.; Kim, J. H.; Allen, E. E.; Venkateswaran, K.;
20 Knight, R. KatharoSeq Enables High-Throughput Microbiome Analysis from Low-
21 Biomass Samples. *mSystems* **2018**, *3*, e00218-17.
- 22
23
24 (111) Stubbins, A.; Dittmar, T. Low Volume Quantification of Dissolved Organic Carbon
25 and Dissolved Nitrogen. *Limnol. Oceanogr. Methods* **2012**, *10*, 347–352.
- 26
27
28 (112) Becker, S.; Aoyama, M.; Woodward, E. M. S.; Bakker, K.; Coverly, S.; Mahaffey, C.;
29 Tanhua, T. GO-SHIP Repeat Hydrography Nutrient Manual: The Precise and Accurate
30 Determination of Dissolved Inorganic Nutrients in Seawater, Using Continuous Flow
31 Analysis Methods. *Front. Mar. Sci.* **2020**, *7*.
- 32
33
34 (113) Hales, B.; Chipman, D.; Takahashi, T. High-Frequency Measurement of Partial
35 Pressure and Total Concentration of Carbon Dioxide in Seawater Using Microporous
36 Hydrophobic Membrane Contactors. *Limnol. Oceanogr. Methods* **2004**, *2*, 356–364.
- 37
38
39 (114) Smith, D.; Azam, F. A Simple, Economical Method for Measuring Bacterial Protein
40 Synthesis Rates in Seawater Using 3H-Leucine. *Mar. Microb. food webs* **1992**, *6*, 107–
41 114.
- 42
43
44 (115) Dinasquet, J.; Tirola, M.; Azam, F. Enrichment of Bacterioplankton Able to Utilize
45
46
47
48
49
50
51
52
53

- 1
2
3 One-Carbon and Methylated Compounds in the Coastal Pacific Ocean. *Front. Mar.*
4 *Sci.* **2018**, *5*, 307.
5
6
7 (116) Asher, E. C.; Dacey, J. W. H.; Jarníková, T.; Tortell, P. D. Measurement of DMS,
8 DMSO, and DMSP in Natural Waters by Automated Sequential Chemical Analysis.
9 *Limnol. Oceanogr. Methods* **2015**, *13*, 451–462.
10
11
12 (117) Levine, N. M.; Varaljay, V. A.; Toole, D. A.; Dacey, J. W. H.; Doney, S. C.; Moran,
13 M. A. Environmental, Biochemical and Genetic Drivers of DMSP Degradation and
14 DMS Production in the Sargasso Sea. *Environ. Microbiol.* **2012**, *14*, 1210–1223.
15
16
17 (118) Gherman, T.; Venables, D. S.; Vaughan, S.; Orphal, J.; Ruth, A. A. Incoherent
18 Broadband Cavity-Enhanced Absorption Spectroscopy in the near-Ultraviolet:
19 Application to HONO and NO₂. *Environ. Sci. Technol.* **2008**, *42*, 890–895.
20
21
22
23
24
25
26
27
28
29
30
31
32
33
34
35
36
37
38
39
40
41
42
43
44
45
46
47
48
49
50
51
52
53

1
2
3
4
5
6
7
8
9
10
11
12
13
14
15
16
17
18
19
20
21
22
23
24
25
26
27
28
29
30
31
32
33
34
35
36
37
38
39
40
41
42
43
44
45
46
47
48
49
50
51
52
53

Tables

| Bloom Cycle | Water Fill Date | Nutrient Addition Date | Nutrient Concentration |
|-------------|-----------------|------------------------|--|
| Bloom 1 | 7/1/2019 | 7/4/2019 | f/2 nutrients + silicates |
| Bloom 2 | 7/12/2019 | 7/14/2019 | f/20 nutrients + silicates |
| Bloom 3 | 7/23/2019 | 7/25/2019 | f/20 nutrients + f/40 silicates |
| | | 7/26/2019 | Addition silicates, to f/20 total |
| | | 8/1/2019 | Additional nutrients and silicates, to total concentration of f/2 for both |

Table 1: Summary of seawater collection and nutrient additions during the three SeaSCAPE bloom cycles.

| Measurement | Technique | Sample type | Sampling Interval | Reference |
|---|---|-------------|---------------------|-----------|
| Dry particle size distributions from 5 nm to 20 μ m | Scanning Mobility Particle Sizer (SMPS, TSI Inc) | N,H,S | 2-5 min | (85) |
| | Aerodynamic Particle Sizer (APS 3321, TSI inc) | N,H | 1 min | (86) |
| | Scanning Electrical Mobility Spectrometer (SEMS, Brechtel) | N,H | 5 min | (87) |
| Total particle number | Condensation Particle Counter (CPC) | N | 1 s | (88) |
| Single particle composition and size | Aerosol Time-of-Flight Mass Spectrometer (ATOFMS) | N,H | 1 min | (89) |
| Size-resolved non-refractory submicron aerosol composition | High Resolution Time-of-Flight Aerosol Mass Spectrometer (HR-ToF-AMS) | N,H,S | 5 min | (40) |
| Ultrafine aerosol chemical composition | Thermal Desorption Chemical Ionization Mass Spectrometer (TDCIMS) | N,S | N: 1 h S: 30 min | (90,91) |
| Submicron aerosol chemical composition | Extractive Electrospray Ionization Mass Spectrometry (EESI-MS) | N,H,S | 1 s | (92) |
| Size-resolved cloud condensation nuclei activity | Continuous-flow streamwise thermal-gradient CCN counter | N,H,S | 30-60 min | (93) |
| Relative humidity-dependent aerosol bounce | Electrical Low Pressure Impactor (ELPI) | N,H,S | 1 min | (94) |
| INP concentration | Continuous-Flow Diffusion Chamber (CFDC) | N,H | 5-15 min | (95) |
| Size-resolved fluorescent biological particle number concentrations | Wideband Integrated Bioaerosol Sensor (WIBS) | N,H | 1 s | (96) |

Table 2: Summary of all online aerosol measurement techniques employed during SeaSCAPE. The sample type is designated by a single letter (N = Nascent SSA, H = Heterogeneously-aged SSA, S = Secondary Marine Aerosol).

| Measurement | Collection Technique | Analysis Technique | Sample type | Sampling Interval | Reference |
|--|----------------------------------|---|-------------|------------------------|-----------|
| INP concentration and characteristics | Polycarbonate filters | Ice spectrometer | N,H | 1-5.5 h | (97) |
| Size-segregated organic aerosol composition | Sioutas cascade impactor | High resolution mass spectrometry | N,H | 6-12 h | (98,99) |
| Single particle morphology, phase state, organic volume fraction, and water uptake | MOUDI impactor | Atomic Force Microscopy (AFM) | N,H | N: 5-6 h H: 1-2 h | (39,100) |
| | | AFM photothermal infrared spectroscopy (AFM-PTIR) | N,H | N: 5-6 h H: 1-2 h | (101) |
| Immersion freezing of single particles | MOUDI impactor | Micro-Raman spectroscopy | N,H | 1-2h | (102) |
| Aerosol pH | MOUDI impactor | pH paper | N | 1-2 h | (103) |
| Chemical and microbial composition | Quartz fiber filters | High-resolution mass spectrometry | N | 24 h | (104) |
| | | 16S/18S rDNA sequencing | N | 24 h | (19) |
| Viral and bacterial abundances | Spot sampler | Flow cytometry | N | 4-6h | (54,55) |
| Enzymes activities | Spot sampler | Fluorogenic substrates | N | 6 h | (59,105) |
| Submicron aerosol speciated organic chemical composition | Quartz fiber filters | TD-GCxGC-EI-HRTof-MS | N | 14 h /10 h (day/night) | (49) |
| Submicron and Supermicron Isotopic Analysis | Cyclone and quartz fiber filters | MAT 253 Isotope-ratio mass spectrometry (IRMS) | N | 48 h | (106) |

Table 3: Summary of all offline aerosol measurement techniques employed during SeaSCAPE. The sample type is designated by a single letter (N = Nascent SSA, H = Heterogeneously-Aged SSA, S = Secondary Marine Aerosol).

| Measurement | Technique | Sample type | Sampling Interval | Reference |
|---|--|-------------|-----------------------------------|-----------|
| O ₃ | UV absorption, Thermo Environmental Model 49C | W,A | 1 s | N/A |
| | UV absorption, 2B Technologies Model 202 | O | 1 s | N/A |
| NO-NO ₂ -NO _x | Chemiluminescence, Thermo Environmental Model 42C | W,A | 1 s | N/A |
| SO ₂ | Pulsed fluorescence, Thermo Environmental Model 43iQ | W,A | 1 s | N/A |
| VOCs | Vocus Proton Transfer Reaction Mass Spectrometry (PTR-ToF-MS) | W,I,A | 1 s | (44) |
| Sulfur-containing VOCs | Chemical Ionization Mass Spectrometry (benzene reagent ion, B-CI-ToF-MS) | I,D | 1 s | (42) |
| Speciated VOC's (Isomer Specific) | TD-GC _x GC-EI-HRToF-MS | I | 20 min collection, every 1-3 days | (46) |
| Abiotic photo-enhanced surface products | Gas phase modified-atmospheric pressure chemical ionization Orbitrap mass spectrometry (APCI-MS) | B,L | 24 h | (45) |

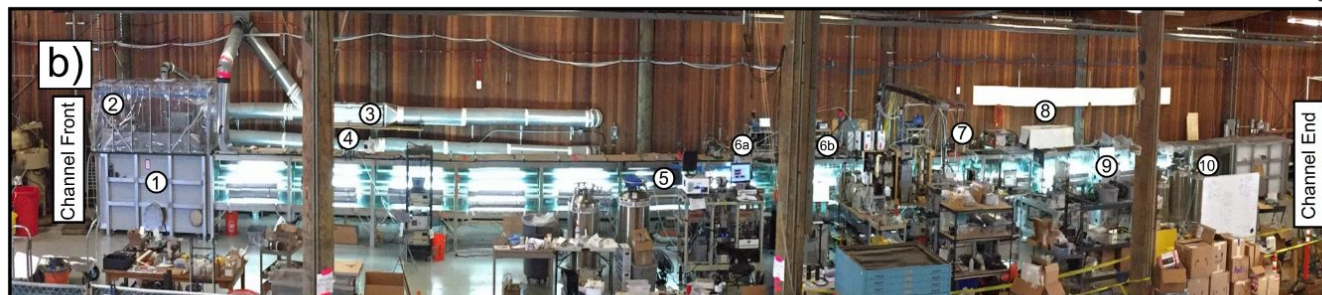
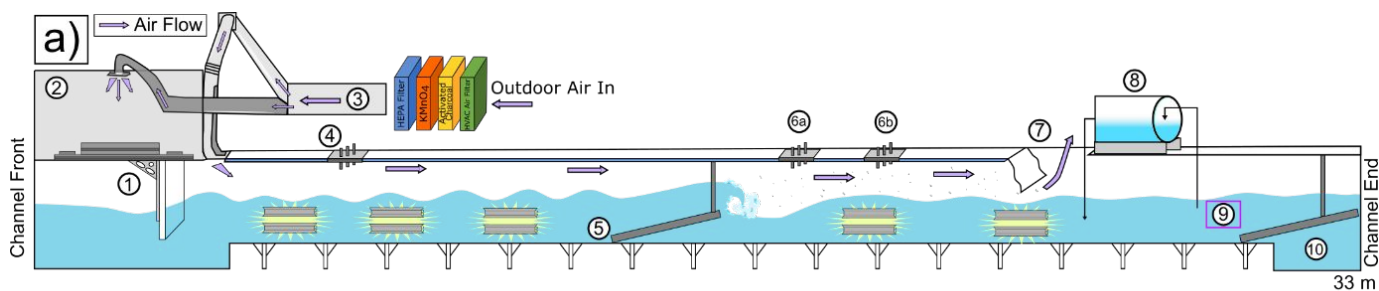
Table 4: Summary of all gas-phase measurement techniques employed during SeaSCAPE. The sample type is designated by a single letter (W = wave channel headspace, I = isolated sampling vessel headspace, D = dissolved gases, A = air handling system, O = OFR, B = bulk seawater, L = SSML).

| Measurement | Technique | Sample type | Sampling Interval | Reference |
|---|--|-------------|-------------------|-----------|
| Chlorophyll-a | Continuous fluorescence (ESP) | B | 1 min | (20) |
| | Fluorescence (AquaFluor) | B | 24 h | (20) |
| | Extracted fluorescence | B | 24 h | (50) |
| Dissolved O ₂ | Continuous optical absorption | B | 1 min | (107) |
| Bacterial community composition | Amplicon Sequencing | B,L | 24 h | (108) |
| Heterotrophic bacteria concentration | Flow Cytometry | B,L | 24 h | (54) |
| Virus concentration | | B,L | 24 h | (55) |
| Nano-pico- phytoplankton and heterotrophic nanoflagellates concentration | | B,L | 24 h | (56,109) |
| Phytoplankton community | <i>In-situ</i> camera | B | 10 Hz | (53) |
| | Microscopy and sequencing | B,L | 24 h | (110) |
| Dissolved organic carbon | High temperature catalytic combustion (Shimadzu TOC-V series instrument) | B | Daily | (111) |
| Speciated DOM organic compounds | HR-ESI-MS | B | 72 h | (80) |
| | TD-GCxGC-EI-HRTof-MS | B,L | 72 h | (49) |
| Nutrients (NO ₃ , NO ₂ , PO ₄ , SiO ₄ , NH ₄) | Seal Analytical continuous-flow AutoAnalyzer 3 | B | 24 h | (112) |

| | | | | |
|--|--|------|---------------------|----------|
| Alkalinity, Bicarbonate, Carbonate, Dissolved Inorganic Carbon, Dissolved CO ₂ , Salinity, pH | Combined pCO ₂ /TCO ₂ Dual Analyzer | B | 1 Hz | (113) |
| Water temperature | Thermocouple (ESP) | B | 1 min | (20) |
| Enzyme Activity | Fluorogenic Substrates | B,L | 24 h | (105) |
| Bacterial production/Growth rate | H3Leucine incorporation | B,L | 24 h | (114) |
| Methylotrophy | C14-methanol incorporation | B,L | 24 h | (115) |
| DMSPp,DMSPd, [DMS]aq | Cryo Purge and Trap Benzene CI-ToF-MS | B | 24 h | (42,116) |
| Functional genes and transcripts dddP, dmdA | Q-PCR for quantification, and sequencing | B, L | 24 h | (117) |
| INP concentration and characteristics | Ice Spectrometer | B,L | 24 h | (97) |
| Fluorescent DOM | Fluorescence excitation emission matrix spectroscopy (EEMS) | B,L | 24 h | (80) |
| HONO production from DOM | Incoherent broadband cavity-enhanced absorption spectroscopy (IBBCEAS) | B | End of Bloom 3 only | (118) |

Table 5: Summary of all seawater and SSML measurements collected during SeaSCAPE. The sample type is designated by a single letter (L = SSML, B = bulk seawater).

Figures



| Wave Channel Location | Distance from Front (m) |
|---|-------------------------|
| ① Reciprocating Paddle System | 0-2.6 |
| ② PTFE Pressure Compensation Tent | 0-2.6 |
| ③ Air Handling Entrance Ports | 0,3,2 |
| ④ Upstream Sampling Port | 6 |
| ⑤ Wave-Breaking Beach | 10.9-13.3 |
| ⑥ Headspace Sampling Ports | 16, 17.5 |
| ⑦ Headspace outlet, PTFE Isolation Film | 20.6 |
| ⑧ Isolated Sampling Vessel | 21.6 |
| ⑨ Bulk Water Sampling Location | 28 |
| ⑩ Wave-Dampening Beach | 29-33 |

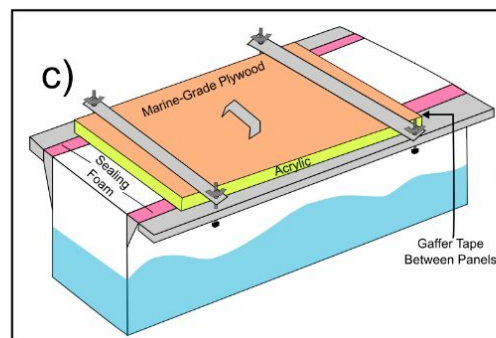


Figure 1. a) Schematic of the SIO Ocean-Atmosphere Interaction Facility (OAIF) wave Channel with key points labeled by number and described in the table, b) Photograph of the SIO OAIF channel with key points marked, c) Cross sectional view of wave channel lids which were used to seal the channel headspace.

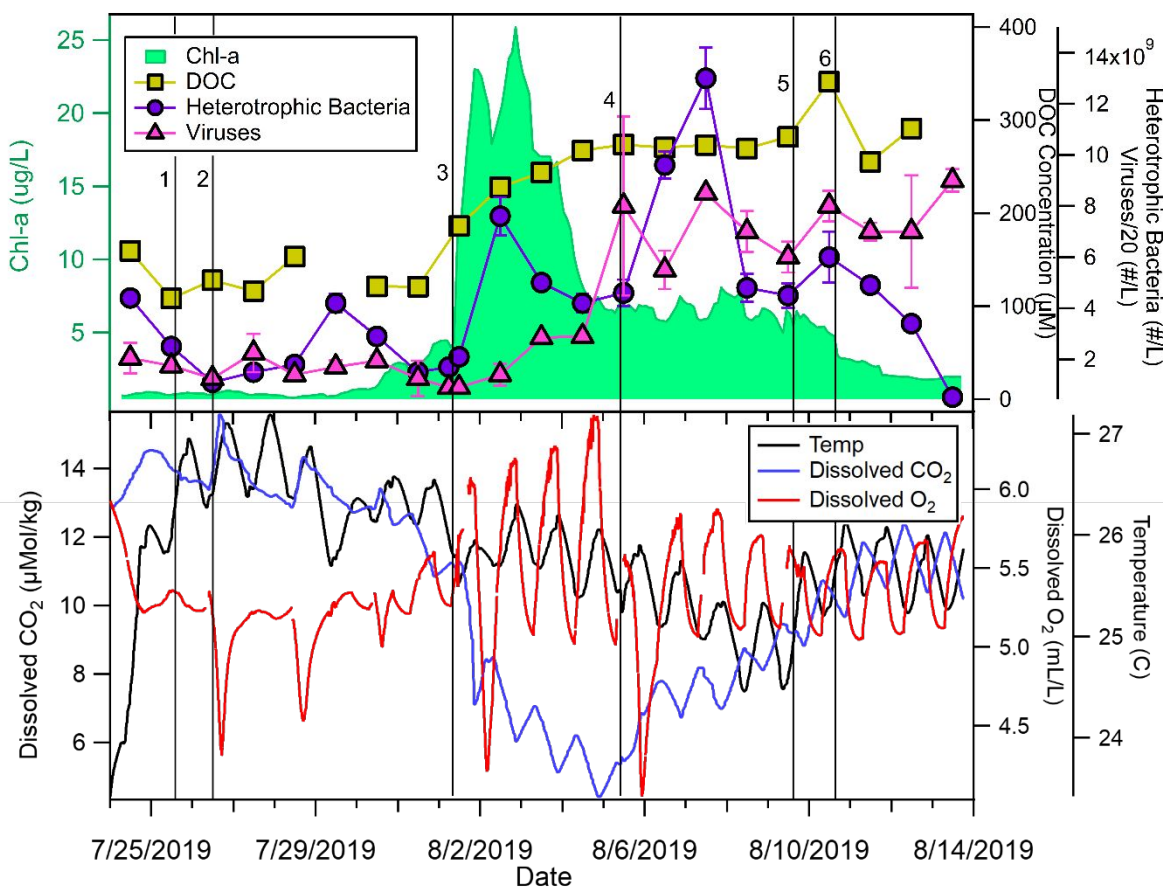


Figure 2. a) SeaSCAPE Bloom 3 chl-a, DOC, heterotrophic bacteria, and virus counts over the mesocosm duration. Numbered vertical lines indicate notable interventions in mesocosm. Lines 1 and 2 correspond to nutrient additions specified in Table 1. Line 3 corresponds to the addition to the wave channel of water from an outdoor tank in which a bloom was induced from the same source water. Line 4 corresponds to the scraping of wave channel walls to remove light-obstructive detritus. Lines 5 and 6 correspond to the addition of circulating pumps to resuspend cellular material that had settled on the wave channel bottom. b) Bloom 3 water temperature, dissolved CO_2 , and dissolved O_2 .

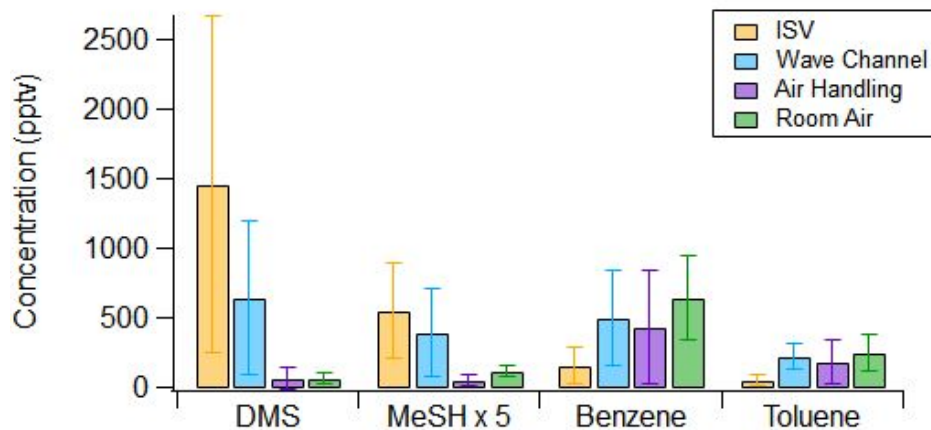


Figure 3. Histogram comparing daytime mixing ratios of DMS, MeSH, benzene, and toluene in the isolated sampling vessel (ISV), wave channel headspace downstream of wave-breaking, air handling system, and hydraulics laboratory room air. Bars show the averages over the entirety of Bloom 3, and error bars represent the 1σ standard deviation over the daily average measurements.

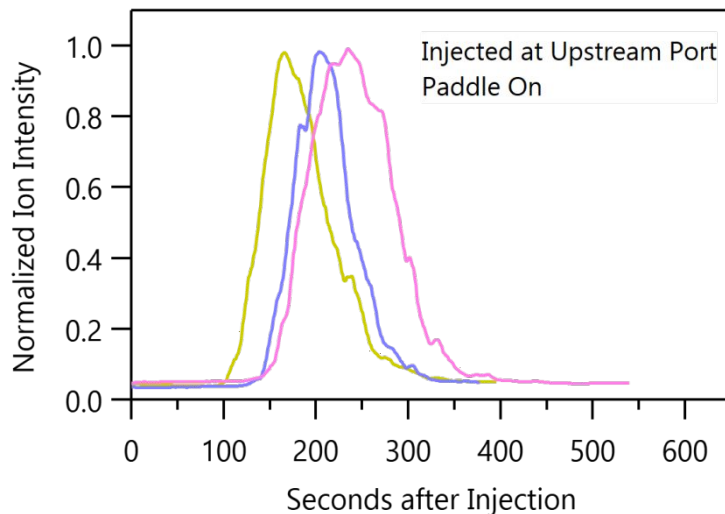


Figure 4. Replicate experiments of dimethyl sulfide (m/z 62) arrival time at the downstream sampling port measured by CI-TOFMS. Instrument signal was boxcar smoothed into 10 second bins. Sample injections were made sequentially on the same day.

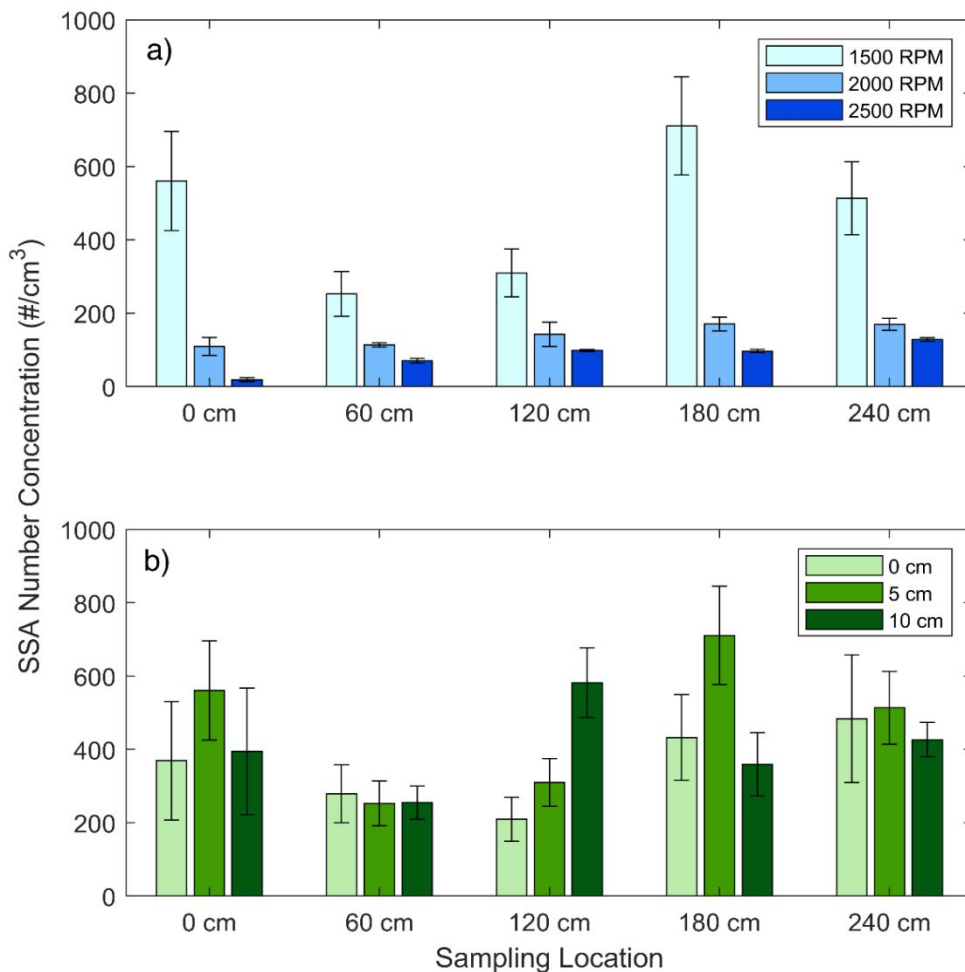


Figure 5. a) SSA number concentration measured at five sampling locations with a 5 cm port depth, testing three different fan settings, which control the air velocity in the wave channel headspace. The lowest setting (1500 RPM) was determined to yield the highest SSA concentrations at all sampling locations. b) The SSA number concentrations at the different sampling locations with a fan speed of 1500 RPM, showing the effect of sampling port depth (0 cm, 5 cm, and 10 cm below the channel lids). There is no clear relationship between sampling port depth or location and number concentration, indicating heterogeneous particle concentrations in the channel headspace. The sampling port locations are evenly spaced and correspond to 0 cm, 60 cm, 120 cm, 180 cm, and 240 cm from the downstream end of the beach.

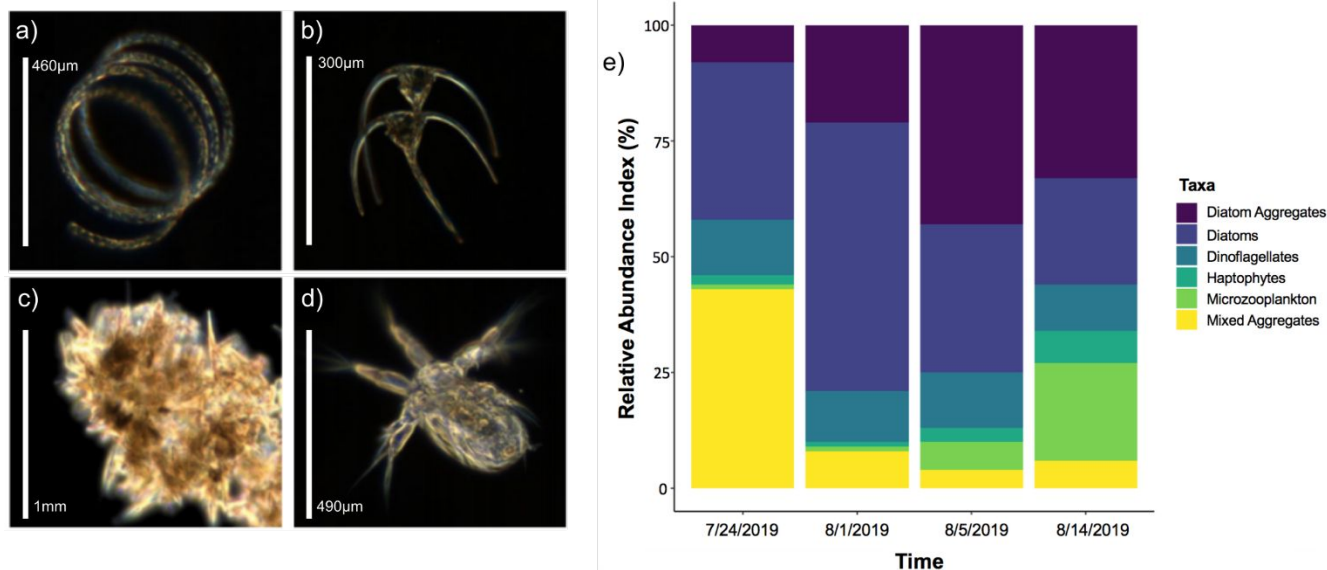


Figure 6. Micrographs of representative taxa across Bloom 3 showing a) diatoms; b) dinoflagellates; c) mixed aggregates (dominated by diatoms and haptophytes); d) nauplius (microzooplankton), e) Time series of relative speciation of phytoplankton taxa across SeaSCAPE.

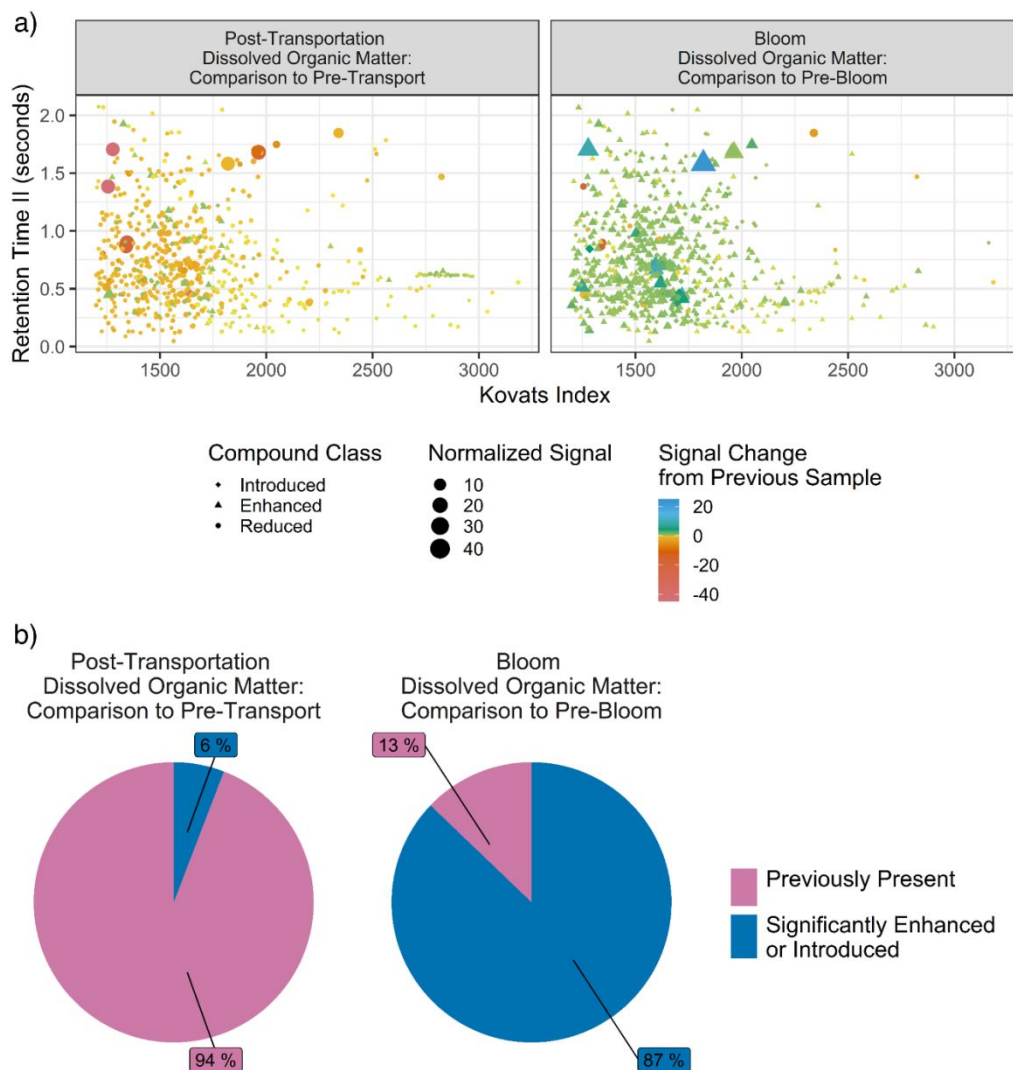


Figure 7. a) Composition of DOM (semi-quantified by internal standard normalized GCxGC ion signal intensity) after physical water transport from Scripps Pier (left) and after introduction of the concentrated bloom addition of 8/1 (right), segregated by change relative to prior sample, with pink indicating signal attributable to previously present compounds and blue attributable to species that are newly introduced or significantly (>15%) enhanced in comparison to the prior signal. a) GCxGC spectra of DOM from Bloom 3, post-transportation

1
2
3 from Scripps Pier into the wave channel (left) and post-bloom addition (right) samples
4 illustrating the relative changes from pre-perturbation conditions. b) Composition of DOM
5 (semi-quantified by internal standard normalized GCxGC ion signal intensity) after physical
6 water transport from Scripps Pier (left) and after introduction of the concentrated bloom
7 addition of 8/1 (right), segregated by change relative to prior sample, with pink indicating
8 signal attributable to previously present compounds and blue attributable to species that are
9 newly introduced or significantly (>15%) enhanced in comparison to the prior signal.
10
11
12
13
14
15
16
17
18
19
20
21
22
23
24
25
26
27
28
29
30
31
32
33
34
35
36
37
38
39
40
41
42
43
44
45
46
47
48
49
50
51
52
53

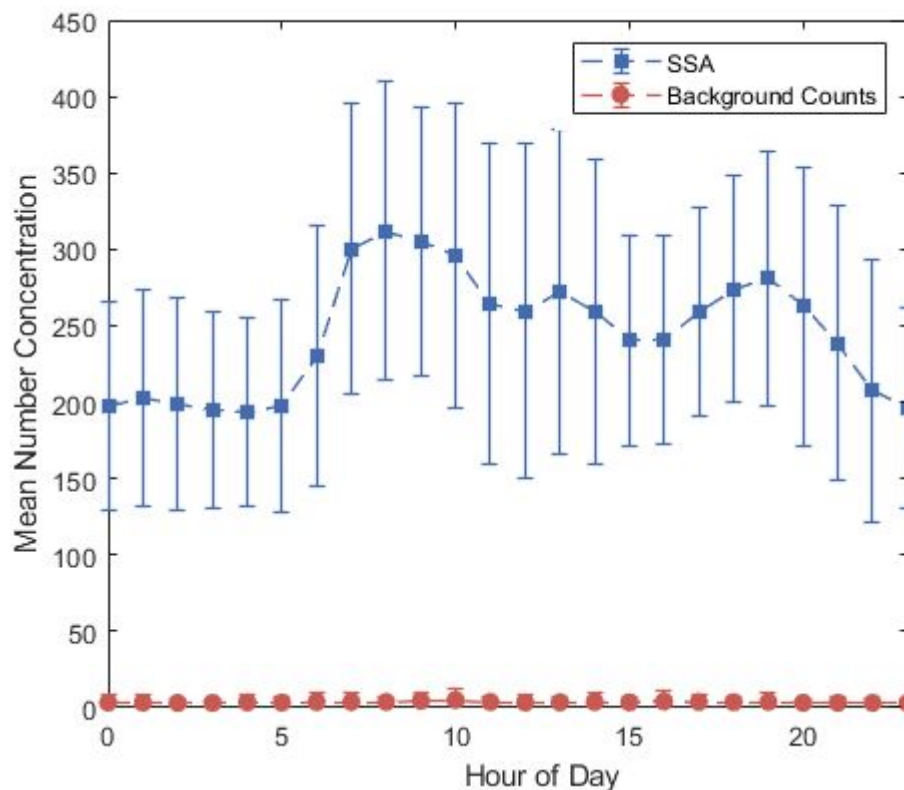


Figure 8. Hourly average SSA number concentrations for all of Blooms 2 and 3, as measured by the APS and SMPS, demonstrating the variability in aerosol production, as well as the observed diurnal behavior. In general, particle concentrations tended to be higher and more variable during the daytime, but lower and more stable overnight. Background particle counts, as measured by the upstream CPC, are also shown. Times reflect local time (PST).

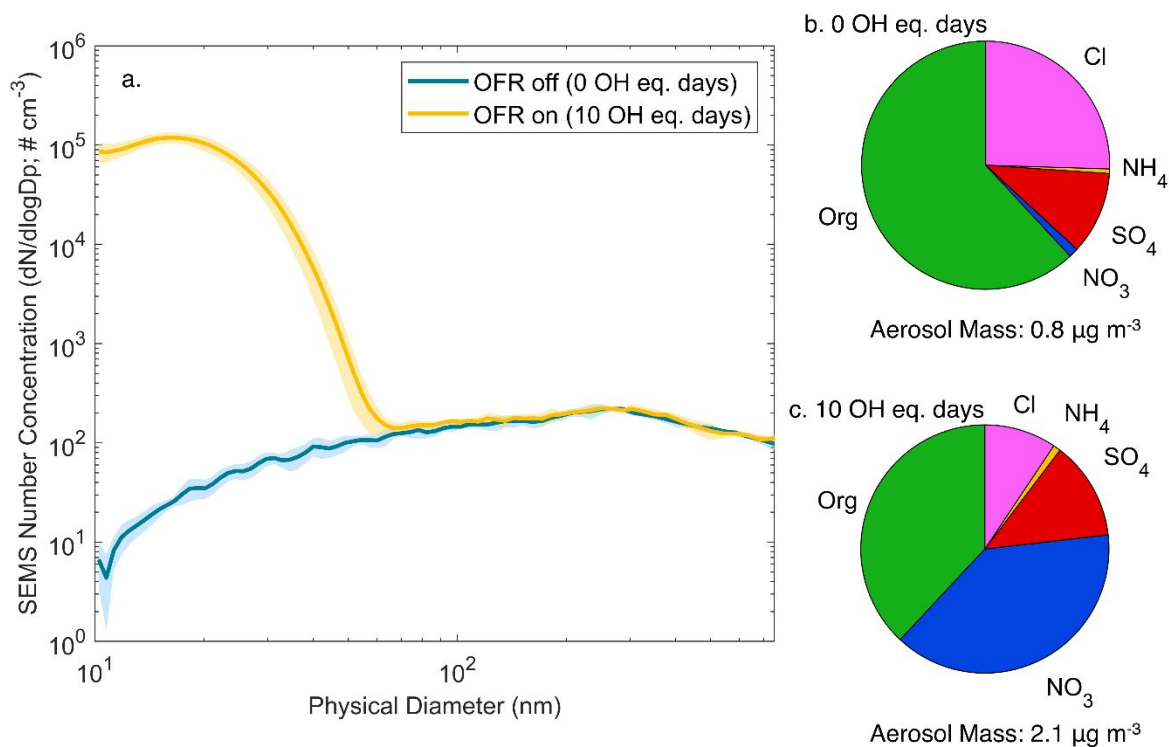


Figure 9. Representative aerosol size distribution from OFR1 (a), in which the complete mixture of gases and SSA from the wave channel headspace are oxidized in the OFR. Shading represents variability in the particle concentrations during the sampling period ($\pm 1\sigma$). The ultrafine mode at <100 nm, which is present only when the lamps are active, is evidence of new particle formation in the reactor. Median fractional bulk chemical composition of submicron non-refractory aerosol, as measured by the AMS, for (b) nascent/bypass SSA and (c) SSA aged 10 OH-equivalent days in the OFR. It is important to note that only a fraction of the total chloride is measured by the AMS.

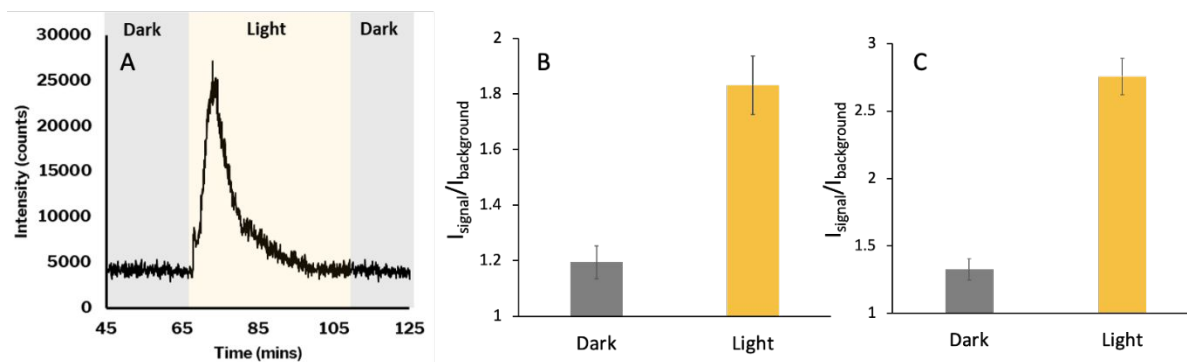


Figure 10. Data from gas-phase APCI high resolution mass spectrometry showing a) total ion current of summed volatile species found to be sensitive to irradiation, where gray indicates when the sample was kept dark and yellow when the sample was subjected to light; b) the signal enhancement of C_6H_6O , likely phenol, upon irradiation, and c) the signal enhancement of $C_{10}H_{16}O$, or beta-cyclocitral, upon irradiation. Error bars represent one standard deviation of the signal averaged over its highest peak.

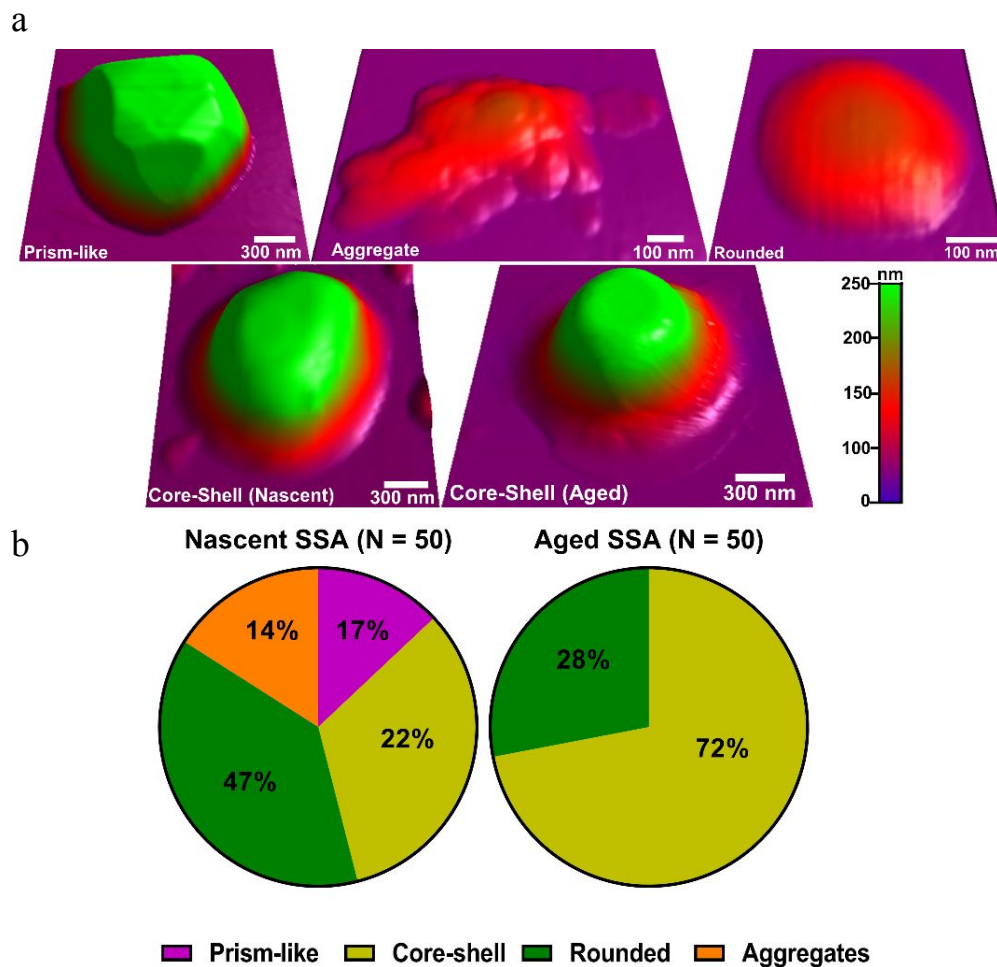


Figure 11. a) Representative AFM 3D-height images of individual SSA particles observed during the peak-bloom (Aug 3rd). Color scale shows height difference between the particles. b) Relative distribution of the morphologies in nascent and aged SSA samples. Prism-like, core-shell, rounded, and aggregates particles are represented by purple, yellow, green, and orange colors, respectively.